Monsalve, A., Yager, E. M., Turowski, J., Rickenmann, D. (2016): A probabilistic formulation of bed load transport to include spatial variability of flow and surface grain size distributions. - *Water Resources Research*, *52*, 5, pp. 3579—3598.

DOI: http://doi.org/10.1002/2015WR017694

AGU PUBLICATIONS

Water Resources Research

RESEARCH ARTICLE
10.1002/2015WR017694

Key Points:
- Including sediment patches improve sediment transport predictions
- Patch and reach averaged shear stress are related through median grain size

Supporting Information:
- Supporting Information S1
- Figure S1
- Figure S2
- Figure S3

Correspondence to:
A. Monsalve,
mons0853@vandals.uidaho.edu

Citation:
Monsalve, A., E. M. Yager, J. M. Turowski, and D. Rickenmann (2016), A probabilistic formulation of bed load transport to include spatial variability of flow and surface grain size distributions, *Water Resour. Res.*, *52*, 3579–3598, doi:10.1002/2015WR017694.

Received 12 JUN 2015
Accepted 9 APR 2016
Accepted article online 20 APR 2016
Published online 13 MAY 2016

A probabilistic formulation of bed load transport to include spatial variability of flow and surface grain size distributions

Angel Monsalve[1,2], Elowyn M. Yager[2], Jens M. Turowski[3], and Dieter Rickenmann[4]

[1]Departamento de Ingeniería en Obras Civiles, Universidad de la Frontera, Temuco, Chile, [2]Department of Civil Engineering, Center for Ecohydraulics Research, University of Idaho, Boise, Idaho, USA, [3]Helmholtz Centre Potsdam, GFZ German Research Centre for Geosciences, Potsdam, Germany, [4]Swiss Federal Research Institute WSL, Mountain Hydrology and Mass Movements, Birmensdorf, Switzerland

Abstract Bed load fluxes are typically calculated as a function of the reach averaged boundary shear stress and a representative bed grain size distribution. In steep, rough channels, heterogeneous bed surface texture and macro-roughness elements cause significant local deviations from the mean shear stress but this variability is often omitted in bed load calculations. Here we present a probabilistic bed load transport formulation that explicitly includes local variations in the flow field and grain size distribution. The model is then tested in a 10% gradient stream, to evaluate its predictive capability and to explore relations between surface grain size sorting and boundary shear stress. The boundary shear stress field, calculated using a quasi-3D hydraulic model, displayed substantial variability between patch classes, but the patch mean dimensionless shear stress varied inversely with patch median grain size. We developed an empirical relation between the applied shear stress on each patch class and the reach averaged shear stress and median grain size. Predicted sediment volumes using this relation in our bed load equation were as accurate as those using complete shear stress distributions and more accurate than current bed load transport equations. Our results suggest that when spatially variable grain size distributions (e.g., patches of sediment) are present they must be explicitly included in bed load transport calculations. Spatial variability in shear stress was relatively more important than grain size variations for sediment transport predictions.

1. Introduction

Mountain rivers with steep slopes (longitudinal gradients greater than 3%) differ from those with lower slopes through a number of characteristics. Such channels are located in headwater catchments, their drainage area is relatively small, and they typically have low discharges and low relative submergences (h/D where h is the average flow depth and D is the characteristic grain size) [*Comiti and Mao*, 2012]. Their channel beds feature wide grain size distributions (GSD) from sand to rarely mobile boulders [*Yager et al*., 2012a] and episodic landslides and debris flows may alter this composition. Additionally, these riverbeds are often composed of patches of sediment, which consist of distinct areas of the bed with relatively narrow GSD and greater sorting compared to the reach [*Laronne et al*., 2000; *Dietrich et al*., 2005]. Patches of sediment affect the flow and boundary shear stress field, the rate and composition of sediment fluxes [*Paola and Seal*, 1995; *Ferguson*, 2003] and can also have biological implications, for instance salmon may find their preferred spawning-sized gravel in zones of finer textures [*Kondolf and Wolman*, 1993; *Buffington and Montgomery*, 1999b; *Buxton et al*., 2015a, 2015b; *Hassan et al*., 2015].

Although sediment patches are common, their formation mechanism is still unclear. When bar morphology or channel obstructions exist, patches can form from topographically induced divergences in boundary shear stress [*Dietrich and Whiting*, 1989; *Lisle et al*., 1991; *Nelson et al*., 2010]. Imbalances in local transport capacity and sediment supply have also been identified as a cause of patch formation [*Dietrich et al*., 1989; *Lisle et al*., 1993, 2000; *Nelson et al*., 2009]. Predicting the formation and location of patches is challenging because of the lack of correlation between local hydraulic properties (e.g., velocity or shear stress) and local surface grain texture [*Lisle et al*., 2000; *Nelson et al*., 2010]. However, most of these correlations were conducted for a single discharge. Shear stress and median grain size could correlate if a range of discharges is considered, or if scales larger than individual grains (e.g., patches) are analyzed. A relation between shear

stress and patch median grain size could also have important consequences for sediment transport predictions.

Sediment patches can lead to large spatial and temporal variations in bed load transport rates, as has been documented in field [*Yager et al*., 2012a; *Segura and Pitlick*, 2015] and laboratory [*Nelson et al*., 2010] measurements and by theoretical modeling [*Lisle et al*., 1993; *Paola and Seal*, 1995; *Ferguson*, 2003; *Chen and Stone*, 2008]. Large relatively immobile boulders, which are a common feature of steep mountain channels, also create a three-dimensional and discharge-dependent flow structure, in which the flow velocity and turbulence intensity can significantly vary [*Comiti et al*., 2007; *Strom and Papanicolaou*, 2007; *Lacey and Roy*, 2008] even in zones not immediately adjacent to the roughness elements, especially in wake zones [*Shvidchenko and Pender*, 2000; *Shamloo et al*., 2001; *Papanicolaou and Kramer*, 2005; *Tritico and Hotchkiss*, 2005; *Ghilardi et al*., 2014; *Hajimirzaie et al*., 2014; *Tsakiris et al*., 2014]. Studies on low gradient rivers have found that spatial-temporal variations of shear stresses are a key factor in determining the areas of the bed that are highly active during sediment transport events [*Segura and Pitlick*, 2015].

Most sediment transport equations are inaccurate in steep streams because they do not include the energy losses or increased total flow resistance caused by macro-roughness elements (e.g., boulders and steps), the limited upstream sediment supply, and the wide GSD that are typical of high gradient channels [*Bathurst et al*., 1987; *Lenzi and D'agostino*, 1999; *Rickenmann*, 2001; *Yager et al*., 2007, 2012b, 2012c; *Mueller et al*., 2008; *Nitsche et al*., 2011; *Schneider et al*., 2015]. Even equations developed for steep channels [e.g., *Smart*, 1984; *Bathurst et al*., 1987; *Graf and Suszka*, 1987; *Aziz and Scott*, 1989] and those that explicitly [*Yager et al*., 2007, 2012c] or implicitly [e.g., *Rickenmann*, 1997, 2005; *Lenzi et al*., 1999; *Nitsche et al*., 2011] account for macro-roughness elements are only accurate to an order of magnitude at best. No investigation has determined if including spatial variability in flow and GSD at a scale smaller than the reach (e.g., patch) can improve bed load transport predictions in steep channels. At the patch scale, local hiding/exposure effects and the relative mobility of different grain sizes may be better captured if the patch's median grain size and local flow conditions are considered instead of those of the reach.

Probabilistic formulations of sediment transport [*Einstein*, 1950; *Paintal*, 1971; *Lisle et al*., 1998] can, theoretically, include the variability of flow and surface texture but their application is generally more difficult than deterministic equations. Probabilistic equations require detailed measurements of flow and bed properties that are not commonly available, or involve extrapolation far beyond the conditions (typically flume experiments) where they were developed. For instance the sediment continuity equations of *Parker et al*. [2000] require functions for the probability of erosion and deposition, which, to date, have not been generalized. The bed load transport equation of *Sun and Donahue* [2000] works well for nonuniform sediment under full motion, but requires the time when a particle is in motion, which has also not been generalized. The use of probabilistic formulations in real field applications is even more unusual. In gravel bed streams, under partial motion conditions, the equation of *Sun and Donahue* [2000] does not perform as well [*Sun and Donahue*, 2000]. However, the field results of *Wu and Yang*'s [2004] fractional transport model suggest that a probabilistic approach has enormous potential.

The objectives of this study are to: (1) investigate whether sediment transport predictions in steep streams are improved when spatial variability in the flow field and grain size, in the form of sediment patches, are explicitly included, (2) explore the correlation between reach and patch averaged shear stresses; and its application in bed load flux predictions, and (3) analyze individual contributions of different patch classes to the total transported sediment volume. To meet our objectives, we use bedload transport, bed conditions and shear stress distributions for a steep stream and develop a new bedload transport formulation.

2. Field Measurements, Sediment Transport Equations and Flow Modeling

Our field work was conducted at the Erlenbach, a steep (10% gradient) stream located in central Switzerland. This stream has been described in detail in several studies [i.e., *Rickenmann*, 1997; *Turowski et al*., 2009; *Nitsche et al*., 2011; *Yager et al*., 2012a, 2012b; *Beer et al*., 2015] and we only focus on characteristics needed for flow modeling and bed load measurements and predictions. Bedload transport rates have been continuously recorded since 1986 using a series of Piezoelectric Bedload Impact Sensors (PBIS) or geophone based bed load impact sensors, both hereinafter called bed load sensors [*Rickenmann and McArdell*, 2007; *Rickenmann et al*., 2012]. The installation, sensitivities and other operating characteristics of these sensors

have been described in detail in several studies [*Rickenmann*, 1997; *Rickenmann and McArdell*, 2007; *Turowski and Rickenmann*, 2011]. Our field site is a 40 m long and 4.7 m wide reach composed of a series of steps, formed by large, relatively immobile boulders, and intervening finer, more mobile sediment patches whose GSD ranges from gravel to cobble [*Yager et al*., 2012a]. The bed load sensors are located directly downstream of our study site, in a steep concrete ramp designed to easily transport all sediment until it reaches a retention basin.

Our field measurement plan was designed to: a) obtain the detailed bed topography, including large roughness elements and banks, b) define each patch class GSD, c) determine the location and area of different patch classes that are potentially active (submerged) during each discharge, and d) estimate reach averaged properties such as step protrusion [*Yager et al*., 2012b].

2.1. Channel Geometry

On 1 August 2010 an extreme event [*Turowski et al*., 2013] rearranged the bed configuration, mobilized boulder steps, increased the in-channel sediment supply [*Yager et al*., 2012b, 2012c], and changed the bed surface packing and armoring. We split our data to account for these changes and conducted measurements during June–July 2010 (hereinafter called 2010 data set) and during July–August 2011 and July 2012 (2011 data set).

We surveyed the bed with a high-resolution ground-based light detection and ranging system (terrestrial LiDAR, Leica ScanStation C10, average point spacing 2 cm) and a total station (Leica-system 1200). Terrestrial LiDAR captured the banks, large boulders, and bed surface above the water level and the total station was used to measure the steps, pools, submerged bed, and any other zones the terrestrial LiDAR was unable to capture (average point spacing of 5 cm). We combined both data sets using AutoCAD® Civil 3D 2014 to obtain a digital elevation model (DEM) that was interpolated, using a linear Kriging algorithm, into a rectangular grid with an average point spacing of 5 cm. The grid size of our numerical simulation ($\sim$10 cm) would not have benefited from a more detailed topography.

2.2. Patch Mapping and Grain Size

Patch boundaries were visually identified as gradual or sharp gradations in GSD and were mapped with the total station. Delineation of patch boundaries has a certain degree of subjectivity [*Nelson et al*., 2014] and one of the same operators was present in all field campaigns to ensure the same criteria was applied. Patches were grouped in different classes following the classification of *Buffington and Montgomery* [1999a], where a certain patch is named based on the relative frequency of the surface grain sizes (gravel (2–64 mm), cobble (64–256), and boulder ($>$256 mm)). Surface grain sizes that occupied less than 5% of the patch area were excluded from the classification. We conducted pebble-counts (counting $\geq$ 100 grains using the grid method on mostly dry patches) on each patch class and divided all patches into immobile (Boulder patches, steps) or relatively mobile sediment [see *Yager et al*., 2012b]. Nine patch classes distributed into 74 individual patches and 6 patch classes with 62 individual patches composed the 2010 and 2011 data set, respectively (Table 1; Figures 1 and 2). The difference between data sets was likely due to bed restructuring and instability after the extreme event of August 2010 [*Turowski et al*., 2013].

2.3. Flow Measurements

We installed 6 and 5 staff plates in different cross sections for the 2010 and 2011 data sets, respectively (Figure 1). We measured water surface elevation (WSE) at each plate throughout 5 and 6 flow events with a total of 8 and 35 measurements for each cross section for the 2010 and 2011 data, respectively. Because of the unsteadiness of the water surface, flow depth (h) at each staff plate was the average of the maximum and minimum h over a period of 60 s. We developed rating curves between h at each cross section and the flow discharge (Q), which is measured at 1 min intervals (stream gage operated by the Swiss Federal Research Institute, WSL [*Nitsche et al*., 2011]) at the downstream end of our reach. For all cross section the average coefficient (R^2) of determination was 0.84 and 0.83 for the 2010 and 2011 data sets, respectively. We tried to simultaneously measure WSE and local flow velocity in each cross section, but even for moderate flows the conditions were too dangerous to wade. We therefore calculated the reach averaged velocity (U) using the method of *Yager et al*. [2012b] (see supporting information for equation and details), which was originally calibrated for our study reach in 2004. The calibration was prior to extreme events in 2007 and 2010 [*Yager et al*., 2012b] and to further ensure that our velocities were in the appropriate range, we

Table 1. Characteristics of Patch Classes for the 2010 and 2011 Data Sets[a]

	2010			2011		
Class	D_{50} (mm)	D_{84} (mm)	A_F	D_{50} (mm)	D_{84} (mm)	A_F
B	522	813	0.25	449	717	0.27
cgB	225	499	0.02	n/p	n/p	n/p
gbC	183	474	0.01	n/p	n/p	n/p
bgC	137	278	0.19	159	291	0.1
C	133	198	0.08	96	142	0.06
bcG	71	268	0.05	n/a	n/a	n/a
gC	64	123	0.21	57	108	0.29
cG	52	103	0.14	50	112	0.18
G	16	29	0.06	20	41	0.10
< 2 mm	n/a	n/a	0.01	n/p	n/p	n/p
Mobile	74	181	0.70	58	141	0.74
Total	117	472	1.00	84	396	1.00

[a]D_{50} and D_{84} are the median and 84[th] percentile grain size for each patch class. A_F is the ratio of the area of each patch class to the entire bed area. "Mobile" represents the bed excluding the immobile steps, "Total" is the entire bed. "n/a" denotes not available and "n/p" is not present. See Figure 2 for patch class definitions and complete GSD.

compared our calculated U (from FaSTMECH, see section 2.4) to those from other resistance equations [*Whittaker*, 1986; *Egashira and Ashida*, 1991; *Pagliara and Chiavaccini*, 2006; *Rickenmann and Recking*, 2011] and to the cross-sectionally averaged velocity ($U_{xs}=Q/A_{xs}$, where the cross-sectional area (A_{xs}) was calculated using the measured cross sections and the $h-Q$ rating curves).

2.4. Flow Modeling and Shear Stress Distributions

We modified *Parker*'s [1990] equations to include the spatially variable boundary shear stress (τ_b) and GSD. To obtain τ_b we used the quasi-3D hydrodynamic model, FaSTMECH, which is included in the iRIC software package V2.3 (www.i-ric.org) and was developed by the U.S. Geological Survey. The model has been described in detail elsewhere [e.g., *Nelson and Smith*, 1989; *Nelson and McDonald*, 1995; *Lisle et al.*, 2000; *Nelson et al.*, 2003; *Mcdonald et al.*, 2005; *Kinzel et al.*, 2009] and used in several studies [*Clayton and Pitlick*, 2007; *Nelson et al.*, 2010; *Conner and Tonina*, 2014; *Maturana et al.*, 2014; *Mueller and Pitlick*, 2014; *Segura and Pitlick*, 2015], so only its major characteristics are mentioned here. The model solves the vertically integrated conservation of mass and momentum equations in a curvilinear grid coordinate system. Approximated vertical velocity profiles are calculated from the two-dimensional (2-D) solution using an assumed eddy viscosity structure [*Rattray and Mitsuda*, 1974]. A zero-equation model for the lateral eddy viscosity, which assumes homogenous and isotropic turbulence, is used for turbulence closure [*Miller and Cluer*, 1998; *Nelson et al.*, 2003; *Barton et al.*, 2005]. The lateral eddy viscosity was constant and equal to 0.005 m^2/s for all our simulated discharges.

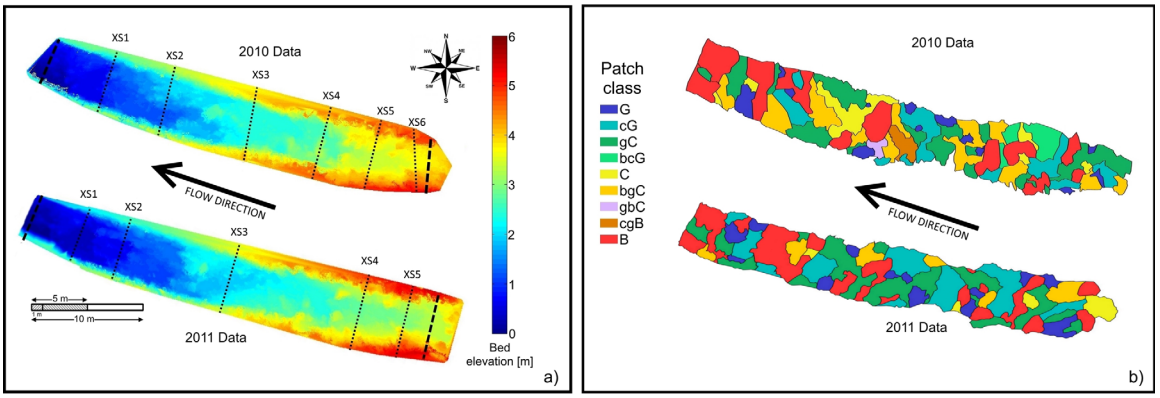

Figure 1. (a) Bed elevation measured before (2010 data) and after (2011 data) the extreme event of 1 August 2010. Bed elevation values were normalized to the lowest elevation at the end of our study reach. The symbol "XS" indicates the locations of the cross sections where WSE were measured. Thick segmented lines indicate the upstream and downstream boundaries of the numerical model. An approach channel (straight trapezoidal channel with a constant streamwise slope) at the upstream boundary was included in the numerical simulations to account for transverse velocity distributions at most-upstream patches. (b) Map of patches within the Erlenbach for the 2010 and 2011 data sets.

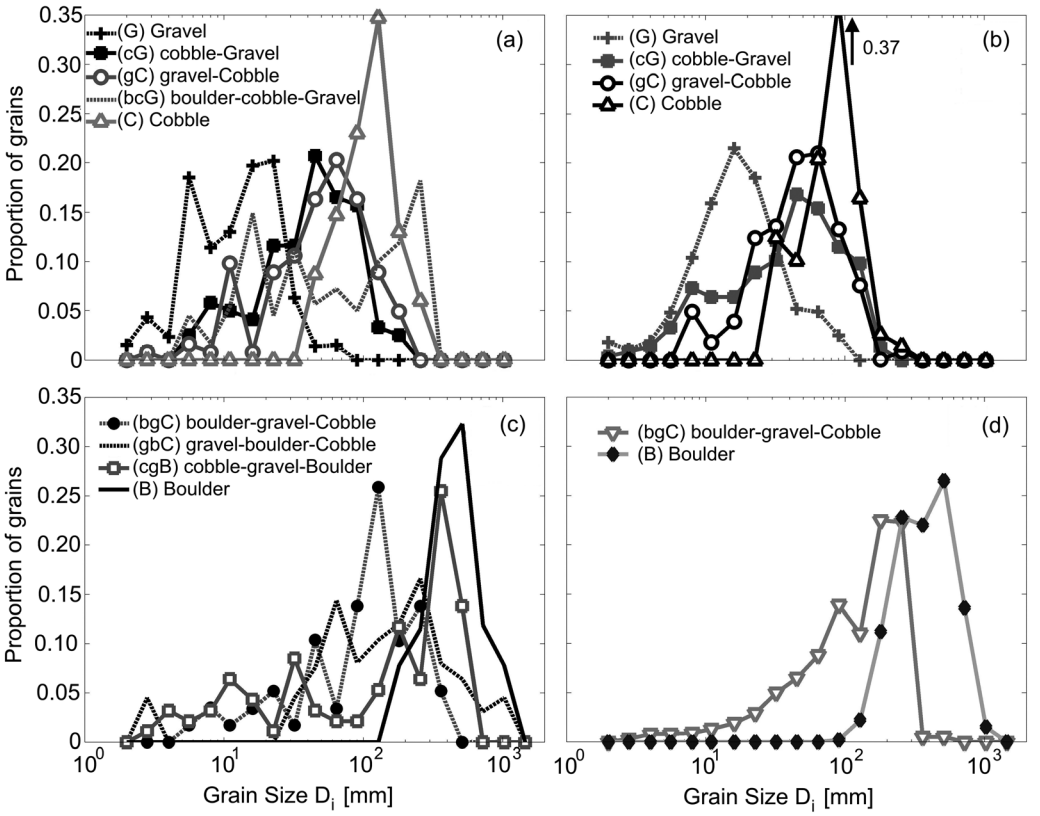

Figure 2. Grain size distributions for each patch class for the two data sets. (a, c) 2010 data and (b, d) 2011 data.

Discharges ranging from 0.10 to 3.5 m^3/s, in increments of 0.05 m^3/s, were simulated to include the entire range of flows during which sediment transport was calculated. Flows below 0.10 m^3/s were not simulated because they produce almost no bed load transport. We used a spatially constant drag coefficient (C_d), that was calibrated for each discharge using the $h-Q$ rating curves and the estimated U from *Yager et al.* [2012b]. The use of a constant C_d can result in similar local shear stresses [*Lisle et al.*, 2000; *Nelson et al.*, 2010] or better predictions of WSE and U [*Segura and Pitlick*, 2015] (see supporting information for more details on C_d). For both data sets (2010 and 2011) C_d (range of 0.12–0.26) varied inversely with depth, which is consistent with the results of *Pasternack et al.* [2006] and *Jarrett* [1984].

The boundary shear stress was calculated at every node (τ_{bn}, where n is a node in the 10 cm mesh, see supporting information section S3) using the model's outputs for the vertically averaged streamwise (u_n) and cross-stream (v_n) velocities,

$$\tau_{bn}=\rho C_d\left(u_n^2+v_n^2\right), \tag{1}$$

where ρ is the water density. Equation (1) was directly computed in FaSTMECH. Two different approaches were used to describe τ_{bn} for a given patch class: a) patch class averaged τ_{bn} (hereinafter "Patch mean"), and b) patch class variable τ_{bn} distribution (hereinafter "Variable distribution"). We could have used individual patches instead of patch classes, but their areas in most cases were often too small to have enough τ_{bn} values (less than 15) to fit probability distributions. For each patch class, data set (2010 or 2011), and discharge we fit five different probability distributions (normal, lognormal, gamma, exponential, and generalized extreme value) to the modeled shear stresses. The normal, lognormal [*Bridge and Bennett*, 1992; *Kleinhans and van Rijn*, 2002], and gamma [*Paola*, 1996; *Nicholas*, 2000; *Bertoldi et al.*, 2009; *Recking*, 2013; *Segura and Pitlick*, 2015] have been used in previous studies and the exponential and generalized extreme value were included to extend our analysis. Parameters in each distribution were estimated using the maximum likelihood estimation (MLE) method and we used the nonparametric test Chi-Square ($\chi 2$) to determine

whether or not the observed shear stresses came from the hypothesized continuous distribution at a 95% significance level. Of those distributions that met the $\chi 2$ test, we selected the one with the highest R^2 from the fit between predicted (from the distribution) and modeled (FaSTMECH) shear stresses. We did this for every discharge and every patch class. If a patch class had less than 15 shear stress values for a given discharge we did not calculate any distribution and bed load transport was determined using the patch class averaged shear stress (see section 2.5). A more detailed analysis of the methods, results and implications of using continuous probability distribution with our probabilistic equations (see section 2.5) is described in supporting information section S4.

2.5. Sediment Transport Equations

Our modified version of *Parker*'s [1990] equations explicitly includes the grain sizes of different patch classes, spatial distribution of shear stresses, and limited sediment supply. The bed was divided into J patch classes that were further divided into N grain size classes with characteristic diameters D_{ij}, where i ranges from 1 to N and j ranges from 1 to J. The geometric mean size (D_{sgj}) and arithmetic standard deviation ($\sigma_{\phi j}$ in ϕ units) for each patch class were calculated as:

$$\ln D_{sgj} = \sum_{i=1}^{N} F_{ij} \ln D_{ij}, \tag{2}$$

$$\sigma_{\phi j}^2 = \sum_{i=1}^{N} \left[\ln \left(\frac{D_{ij}}{D_{sgj}} \right) (\ln 2)^{-1} \right]^2 F_{ij}, \tag{3}$$

where F_{ij} is the volume fraction of the i^{th} grain-size class in the j^{th} patch class . The local applied dimensionless shear stress (τ^*_{sgj}, hereinafter the superscript * denotes a dimensionless quantity) at the j^{th} patch class was calculated as:

$$\tau^*_{sgj} = \frac{\tau_{bnj}}{\rho R_s g D_{sgj}}, \tag{4}$$

where τ_{bnj} is a local applied shear stress at the j^{th} patch class, R_s is the dimensionless submerged specific gravity of sediment and g the acceleration due to gravity. Hereinafter we refer to τ^*_{sgj} simply as τ^*_j. For sediment transport, the only relevant locations were where the local dimensionless shear stress was higher than the dimensionless critical shear stress (assumed $\tau^*_c = 0.045$ [*Buffington and Montgomery*, 1997]); we only used locations in which $\tau^*_j \geq \tau^*_c$. Although the smaller fractions of fine sediment patches could be in motion for these low shear stresses, their contribution to the total transported volume was negligible and neglecting low τ^*_j allowed us to simplify our calculations. The probability density function ($P_{\tau^*_j}$, see Figure 3 for definitions) of τ^*_j follows the best-fit distribution that may change with the discharge. The lower, τ^*_{jl}, and upper, τ^*_{ju}, limits of the distribution were set as the 1st and 99th percentile of the best-fit distribution. Bedload transport rates were calculated at discrete intervals of τ^*_j, where the width of each interval ($\Delta\tau^*_j$) is given by:

$$\Delta\tau^*_j = \frac{\tau^*_{ju} - \tau^*_{jl}}{K}, \tag{5}$$

with $K = 25$ as the number of intervals. Since the patch mean approach does not require a discrete interval, τ^*_j is simply the average of all shear stresses for each discharge and patch class. Within a patch class the fraction of the bed area, A_{jk}, where a certain τ^*_j acts is:

$$A_{jk} = \Delta\tau^*_j P_{\tau^*_j}, \tag{6}$$

with k ranging from 1 to K, therefore the τ^*_j acting on A_{jk} is defined as τ^*_{jk}. The process for calculating τ^*_j, A_{jk} and τ^*_{jk} is shown in Figure 3. The hiding function (ϕ_{ijk}) for the k^{th} subregion in the j^{th} patch class is:

$$\phi_{ijk} = \omega_{jk} \phi_{sgojk} \left(\frac{D_{ij}}{D_{sgj}} \right)^{-\beta}, \tag{7}$$

where ϕ_{sgojk} is:

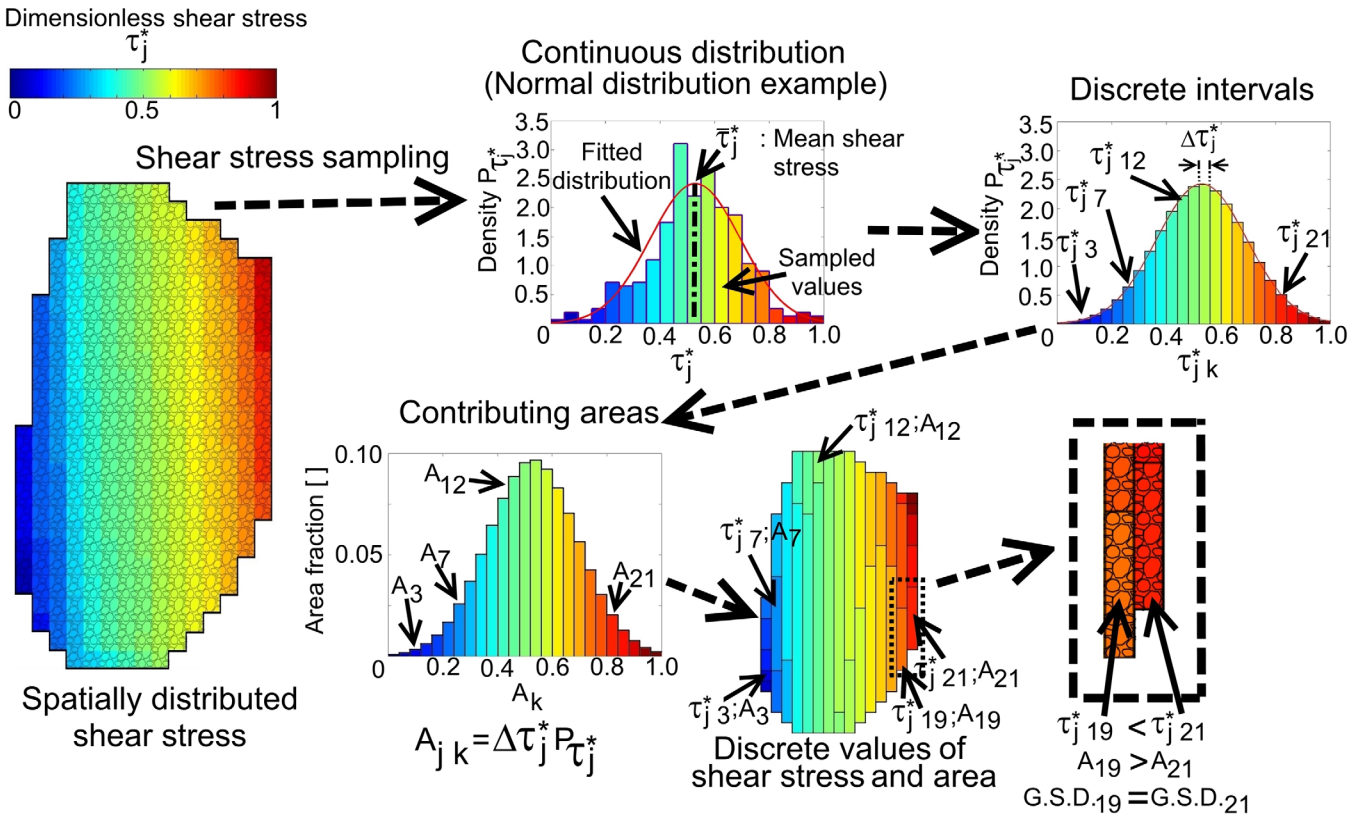

Figure 3. Diagram of the process to calculate discrete shear stresses from spatially distributed values. The process starts with sampling the spatial variations of shear stresses over a patch class (first figure at left) and then the observed shear stress distribution is simplified assuming that it comes from a probability distribution. For simplicity a single patch is shown in the figure although in our analysis we used patch classes. The process is repeated for each patch class and every given discharge. Definitions used in equations (5) and (6) are graphically represented.

$$\phi_{sgojk}=\frac{\tau_{jk}^*}{\tau_{rsgo}^*}, \tag{8}$$

The exponent β is 0.16 for all patch classes and was calculated using tracer particles installed in our reach [*Yager et al.*, 2012b] and τ_{rsgo}^* is a dimensionless reference stress (0.0386, in the original *Parker* [1990] equation). A sensitivity analysis of the bed load transport predictions to this hiding function is provided in supporting information section S5). The empirical function ω_{jk} is defined as:

$$\omega_{jk}=1+\frac{\sigma_{\phi j}}{\sigma_{\phi 0}\left(\phi_{sgojk}\right)}\left(\omega_0\left(\phi_{sgojk}\right)-1\right), \tag{9}$$

where $\sigma_{\phi 0}\left(\phi_{sgojk}\right)$ and $\omega_0\left(\phi_{sgojk}\right)$ are graphical functions from *Parker* [1990]. The dimensionless bed load transport rate W_{sijk}^* for each i^{th} size class in for each k^{th} subregion on the j^{th} patch class is:

$$W_{sijk}^*=0.00218G\left(\phi_{ijk}\right), \tag{10}$$

where

$$G\left(\phi_{ijk}\right)=\begin{cases}5474\left(1-\dfrac{0.853}{\phi_{ijk}}\right)^{4.5}, & \phi_{ijk}>1.59\\ \exp\left[14.2\left(\phi_{ijk}-1\right)-9.28\left(\phi_{ijk}-1\right)^2\right], & 1\le\phi_{ijk}\le 1.5,\\ \phi_{ijk}{}^{14.2}, & \phi_{ijk}<1\end{cases} \tag{11}$$

The volumetric transport rate per unit width (q_{ijk}) for the i^{th} size class in the k^{th} subregion on the j^{th} patch class:

$$q_{ijk}=\frac{\left(\frac{\tau_{jk}}{\rho}\right)^{1.5}F_{ij}\,W^*_{sijk}}{R_s g}A_{jk}, \tag{12}$$

The volumetric transport rate per unit width for each i^{th} size class on the j^{th} patch class is:

$$q_{ij}=\sum_{k=1}^{K}q_{ijk}, \tag{13}$$

and the volumetric transport rate per unit width for the j^{th} patch class is $q_j=\sum_{i=1}^{N}q_{ij}$. The total transport rate per unit width (q_T) is:

$$q_T=\left(\sum_{j=1}^{J}q_j\frac{A_j}{A_{Tw}}\right)\frac{A_m}{A_T}Z^*_m, \tag{14}$$

where A_j is the wetted, or submerged, bed area of the j^{th} patch class, A_{Tw} is the total wetted bed area, A_m is the area fraction occupied by relatively mobile grains (i.e., the bed excluding immobile steps) and A_T is the total bed area. The ratio A_j/A_{Tw} is a weighting factor that accounts for the individual contributions of each patch class to the total bed load. Z^*_m is the ratio of the mobile sediment deposit thickness at the time of an individual flow event (Z_t) to that immediately after the last extreme event (Z_{t0}).

$$Z^*_m=\frac{Z_t}{Z_{t0}}, \tag{15}$$

If the mean immobile-grain diameter (D_I) does not vary with time (t, in units of months, see supporting information for details) then Z^*_m can be approximated as:

$$Z^*_m=\frac{1}{0.85}\left(1-0.15t^{0.21}\right), \tag{16}$$

The upstream sediment supply, which is typically limited in steep streams, is included by scaling the predicted total transport rate by the volumetric proportion of the bed covered by relatively mobile sediment, $(Am/A_T)Z^*_m$. This scaling factor was based on the observations of *Yager et al.* [2007] in which the immobile grain protrusion varied with sediment supply. Later, *Yager et al.* [2012c] showed that step protrusion was a proxy for sediment supply at any given time given that it increased with greater time elapsed since an extreme event, which are associated with high sediment supplies [*Turowski et al.*, 2009]. The ratio Am/A_T changed between the two data sets (0.70 and 0.74 for the 2010 and 2011 data sets, respectively), but it was assumed constant within each set.

2.6. Sediment Flux Measurements and Predictions

Our transport predictions depend on bed topography, patch class GSD, and assumed relative sediment supply, which in turn depend on the time elapsed since the last extreme event. The last recorded extreme events occurred on 20 June 2007 and 1 August 2010 [*Turowski et al.*, 2009, 2013], and therefore we limit our analysis to events after 2007. The bed load sensors were not calibrated for low sediment yield events [*Rickenmann and McArdell*, 2007], and all events with less than 3 m^3 of transported sediment were excluded from our analysis (~37% of the events). In addition, events containing discharges larger than 9 m^3/s (the two extreme events) were also omitted for two reasons: (i) there are likely large uncertainties in extrapolating our WSE to those high discharges, and (ii) the WSE is likely outside our numerical domain boundaries (overbank flow). Measured transported volumes were corrected for porosity (assumed 40%) (details on measured transport in *Rickenmann and McArdell* [2007]; *Rickenmann et al.* [2012]; *Yager et al.* [2012b]). Although our simulations do not cover all possible individual discharges throughout each hydrograph (see section 2.4), they bracket the measured values. To obtain q_{ij} and A_j for any specific discharge within the measured hydrograph we used spline cubic interpolations between known values. We did not analyze if modifications to sediment transport equations other than the *Parker* [1990] equation would further improve predictions (but see *Schneider et al.* [2015] for accuracy of other equations).

3. Results

3.1. Hydrodynamic Model Simulations and Results

Water surface elevation RMSE (root mean squared error) for our simulated discharges was 0.06 m (standard deviation (std) 0.06 m; 10% of mean flow depth) and 0.04 m (std 0.04 m; 7% of mean flow depth) for the 2010 and 2011 data, respectively. The RMSE of the reach-averaged velocity from the hydrodynamic model versus the *Yager et al*. [2012b] method, for both data sets was 0.014 m/s. The equation of *Ferguson* [2007] that uses the coefficient from *Rickenmann and Recking* [2011], gave similar velocities, although slightly larger, to those predicted by the hydrodynamic model (differences of 5–9% and 2–8% for the 2010 and 2011 data sets). This similitude between velocities confirms the successful calibration of our hydrodynamic model (Figure 4). The equations of *Whittaker* [1986], *Egashira and Ashida* [1991], and *Pagliara and Chiavaccini* [2006] gave larger velocities than *Rickenmann and Recking* [2011], *Yager et al*. [2012b], and the hydrodynamic model.

The RMSE between the model's cross-sectionally averaged velocity (hereinafter $U_{xs\,model}$) and U_{xs} for the 2010 and 2011 data sets were 0.081 and 0.076 m/s, respectively. The major differences between $U_{xs\,model}$ and U_{xs} were observed at high discharges (approximately over 1.5 m/s) and could be partly arise from uncertainties of (i) the stage-discharge and $h-Q$ relations, where fewer calibration measurements for higher discharges exist, (ii) the hydrodynamic model's simplifications of governing equations, (iii) assuming a constant C_d, and (iv) the use of constant cross section geometries for U_{xs} that may not have been perpendicular to the local flow at all discharges.

3.2. Patch and Reach Averaged Shear Stress

To study the correlation between (τ_{bn}, grid scale) and local grain size we conducted an analysis similar to that of *Lisle et al*. [2000]. We did not have a detailed map of the local median grain size (i.e., at a subpatch scale) and used the patch class median grain size (D_{50j}) instead. We obtained a very low coefficient of determination between τ_{bn} and D_{50j} (R^2=0.23, α= 0.05, Figure 5a), which confirms the results of *Lisle et al*. [2000] and *Nelson et al*. [2010]. However, the patch class averaged shear stress ($\bar{\tau}_j$) varied directly with D_{50j} for a given discharge (Figure 5b).

Although we use the patch-scale shear stress, the reach averaged dimensionless shear stress ($\bar{\tau}^*$) is typically used for bed load transport calculations. We tested how $\bar{\tau}^*$ varied using two different calculation methods (Figures 6a and 6b): (i) First, the mean dimensionless shear stress for each patch class ($\bar{\tau}_j^*$) was a function of the mean shear stress of each patch class ($\bar{\tau}_j$) normalized by the median grain size (D_{50j}) of that patch class and then $\bar{\tau}^*$ was the patch class area (only wetted portion) weighted average of all $\bar{\tau}_j^*$ and is hereinafter called $\bar{\tau}^*_{var\,D_{50}}$. (ii) Second, $\bar{\tau}^*$ was calculated in almost the same way but is instead normalized using the reach-averaged surface median grain size (D_{50}), which is normally done in the literature. The entire area of each patch class was used instead of just the wetted area and this method is called $\bar{\tau}^*_{cst\,D_{50}}$. For any given discharge and for both data sets, $\bar{\tau}^*_{cst\,D_{50}}$ was lower than $\bar{\tau}^*_{var\,D_{50}}$ (Figure 6a) because of the use of a single D_{50} and patch area in $\bar{\tau}^*_{cst\,D_{50}}$. Although $\bar{\tau}^*_{cst\,D_{50}}$ was not used in our bed load transport calculations, it shows that the patch class-scale D_{50j} can significantly impact the reach-averaged shear stress.

We also calculated the shear stress acting on the potentially mobile sediment ($\bar{\tau}_m^*$), using the shear stress partitioning method of *Yager et al*. [2012b, 2012c], to compare to $\bar{\tau}^*_{var\,D_{50}}$. This method accounts for immobile grain drag to indirectly reduce the shear stress on mobile patches whereas our hydrodynamic model includes the flow divergence caused by boulders to directly affect the shear stress on mobile patches. For most discharges and both data sets, $\bar{\tau}^*_{var\,D_{50}}$ was lower than $\bar{\tau}_m^*$, with percent differences as high as 50% for large discharges (Figure 6b). However, within the discharge range where most sediment transport occurs (based on a magnitude frequency analysis, light gray area in Figure 6b, see *Nitsche et al*. [2011]), both methods predict similar dimensionless shear stresses for a given discharge, indicating that $\bar{\tau}_m^*$ can roughly capture the effects of boulders on shear stress. Our results are slightly different from *Segura and Pitlick* [2015] who demonstrated that the differences between mean shear stress from a 2-D flow model and the total shear stress (slope-depth product) decreased with increasing flow.

Our model captured significant spatial variability in shear stress that was not represented by the approach of *Yager et al*. [2012b] (Figure 6c). The coefficient of variation in $\bar{\tau}^*_{var\,D_{50}}$ (CV), defined as the ratio of the standard deviation to the mean value, was fairly constant for both data sets.

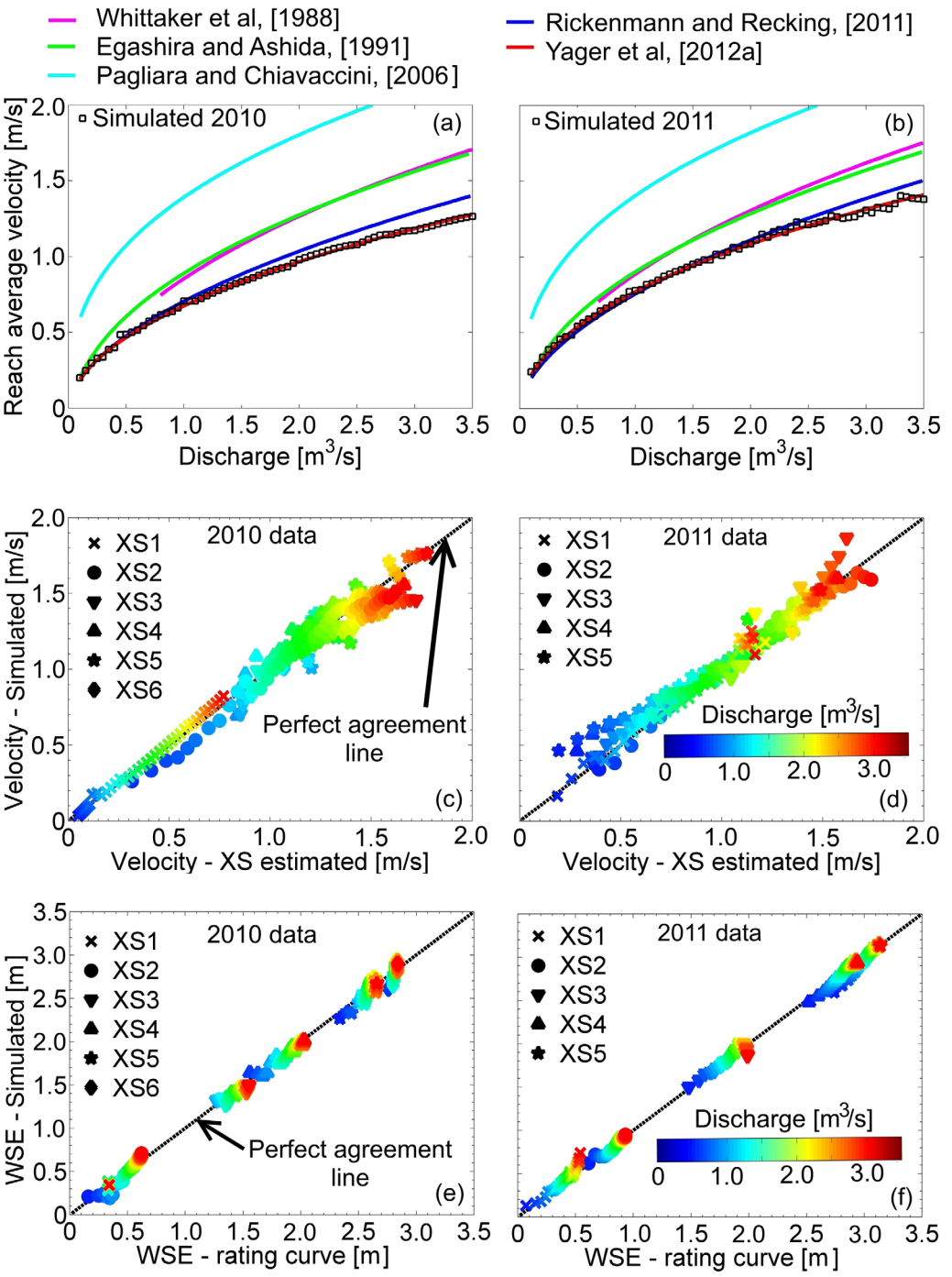

Figure 4. Reach averaged velocities for the (a) 2010 and (b) 2011 data sets predicted by the hydrodynamic model compared to those predicted by *Yager et al.* [2012b] as functions of discharge. Predictions from the resistance equations of *Whittaker* [1986], *Egashira and Ashida* [1991], *Pagliara and Chiavaccini* [2006], and *Rickenmann and Recking* [2011] (see text for details and description) are shown for comparison. Cross-sectionally averaged velocities for the (c) 2010 and (d) 2011 data sets predicted by the hydrodynamic model compared to those from our field measurements, where XS means cross section. Each velocity point is colored by its corresponding discharge.

3.3. Predictions of Sediment Flux

We used three different approaches (see section 2.4) to calculate bed load transport: (i) Patch mean; (ii) Variable distribution; and (iii) *Yager et al.* [2012c], which uses a single shear stress for a given discharge and does not include the effect of patches (Figure 7, method Shear stress – grain size relation within this figure is explained later in section 3.4). Predictions of sediment transport for each of the 43 tested events (36 and

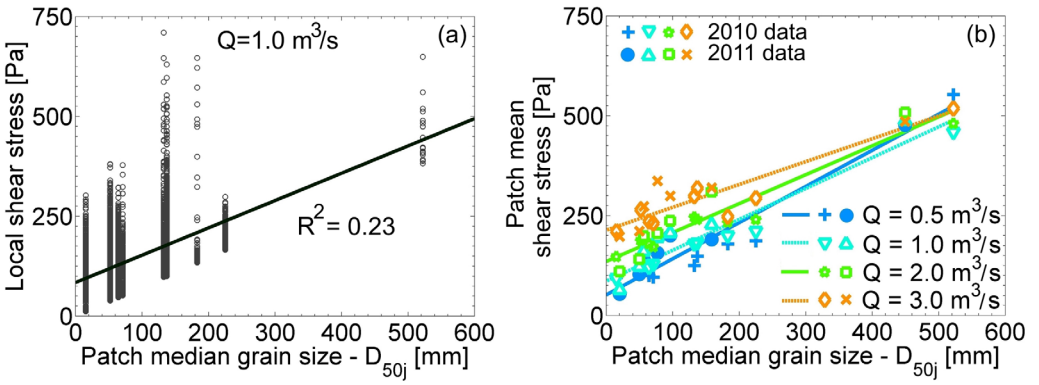

Figure 5. (a) Local boundary shear stress versus patch median grain size for a discharge of 1 m^3/s for the 2010 data set. The same results were found for discharges of 0.5, 2.0, and 3.0 m^3/s, which cover most of our studied discharge range. Each circle represents a wetted node in the numerical model. (b) Patch class averaged shear stress as a function of the patch class median grain size for different discharges. Linear fits are included to help visualize the trend, but they do not necessarily represent the best possible fit.

7 for 2010 and 2011, respectively) used the bed topography (and associated shear stresses) for that time period. If an event occurred before or after the extreme event of August 2010, we used the 2010 or 2011 data sets, respectively. Bedload volumes calculated using the "Patch mean" approach were always within one order magnitude of the measured values, had the lowest RMSE (m^3), and did not systematically over or under predict the measured volumes (Figure 7). 53% of all events for the "Patch mean" approach had a ratio of the predicted to the measured transported volumes between 0.5 and 2 (factor of 2). The "Variable distribution" approach produced similar results for the bulk of the measured events, but the volume of one event was overpredicted by over an order magnitude (Figure 7). We chose the *Yager et al.* [2012c] method to compare to the performance of the "Patch mean" and "Variable distribution" approaches because: (a) it was already tested in exactly the same reach, and (b) it has relatively accurate predictions to compare against those of our equation.

The *Yager et al.* [2012b] approach had about double the RMSE (99 m^3) than the "Patch mean" (40 m^3) and "Variable distribution" (51 m^3) approaches. For all three approaches most sediment transport events were overpredicted ("Patch mean" 58%; "Variable distribution": 65%; *Yager et al.* [2012b]: 63%) rather than underpredicted (Table 2).

3.4. Grain Size and Shear Stress Relation

Although bed load transport predictions using the "Patch mean" method are more accurate than those using *Yager et al.* [2012c], they rely on very detailed topographic information not commonly available for most rivers. A more broadly applicable equation that empirically includes the effects of patch classes is therefore desired. Given that patch class mean shear stress on the j^{th} patch class ($\bar{\tau}_j$) increases with patch median grain size (D_{50j}) (Figure 5b), we analyzed if this relationship could be used in our sediment transport equation. Since the reach-averaged shear stress ($\bar{\tau}$) in steep rough channels can be easily estimated using flow resistance partitioning techniques [e.g., *Comiti et al.*, 2007; *Yager et al.*, 2007, 2012b; *Nitsche et al.*, 2011; *Rickenmann and Recking*, 2011], we developed a function that relates $\bar{\tau}_j$ to D_{50j} and $\bar{\tau}$. Two different approaches were used to define $\bar{\tau}$ for all discharges: (i) $\bar{\tau}_{var\,D50}$ as discussed in section 3.2 and (ii) total shear stress ($\bar{\tau}_T$) defined ρghS (where S is the average bed slope) which is the most accessible flow parameter used in sediment transport predictions.

We used a power law to relate $\bar{\tau}_j$ to $\bar{\tau}$,

$$\bar{\tau}_j = c_p \bar{\tau}^{e_p} \tag{17}$$

where the R^2 was 0.75 for both $\bar{\tau}_{var\,D_{50}}$ and $\bar{\tau}_T$. The coefficient (c_p) and exponent (e_p) of equation (17) varied with the dimensionless median grain size D_{50j}/D_{50} (Figures 8a and 8b). When using $\bar{\tau}_{var\,D50}$ a power law and a logarithmic relation with respect to D_{50j}/D_{50} 83% and 75% of the variability in c_p and e_p were explained, respectively (Figures 8a and 8b),

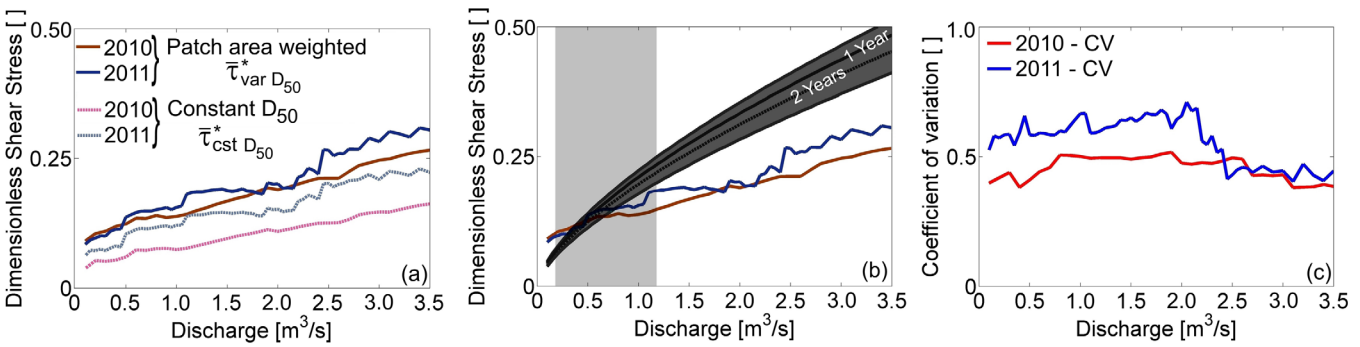

Figure 6. (a) Dimensionless reach-averaged shear stress dependence on the median grain size used for normalization ($\bar{\tau}^*_{var\ D_{50}}$ and $\bar{\tau}^*_{cst\ D_{50}}$ methods, shear stresses calculated from hydrodynamic model). (b) Reach averaged dimensionless shear stresses predicted by the hydrodynamic model ($\bar{\tau}^*_{var\ D_{50}}$) for both data sets as functions of discharge compared to those predicted by the shear stress partitioning method of *Yager et al.* [2012b]. The dark grey area represents four different step protrusions calculated at 0.5, 1, 2, and 5 years since an extreme event. Upper and lower limits correspond to 0.5 and 5 years respectively, whereas 1 and 2 years are labeled directly. The light grey area shows the discharges where 90% of the sediment transport occurred for our events, calculated using a magnitude frequency analysis based on the sediment transport events from June 2007 until September 2010 using a total of 4494 individual discharges. (c) The coefficient of variation of the dimensionless reach averaged shear stress ($\bar{\tau}^*_{var\ D_{50}}$) as a function of discharge.

$$c_p = 5.31\left(\frac{D_{50j}}{D_{50}}\right)^{2.52}, \quad \bar{\tau} = \bar{\tau}_{var\ D_{50}} \tag{18a}$$

$$c_p = 6.52\left(\frac{D_{50j}}{D_{50}}\right)^{2.46}, \quad \bar{\tau} = \bar{\tau}_T \tag{18b}$$

$$e_p = -0.37\ln\left(\frac{D_{50j}}{D_{50}}\right) + 0.70, \quad \bar{\tau} = \bar{\tau}_{var\ D_{50}} \tag{19a}$$

$$e_p = -0.33\ln\left(\frac{D_{50j}}{D_{50}}\right) + 0.61, \quad \bar{\tau} = \bar{\tau}_T \tag{19b}$$

We analyzed the performance of equations (17)–(19) (hereinafter called $\bar{\tau}_j - \bar{\tau} - D_{50j}$) by comparing their predicted $\bar{\tau}_j/\bar{\tau}$ to the actual hydrodynamic model results (Figure 8c). The average R^2 between the predicted and measured $\bar{\tau}_j/\bar{\tau}$ was 0.92 and 0.90 ($\alpha = 0.05$) for $\bar{\tau}_{var\ D_{50}}$ and $\bar{\tau}_T$, respectively. Therefore the $\bar{\tau}_j - \bar{\tau} - D_{50j}$

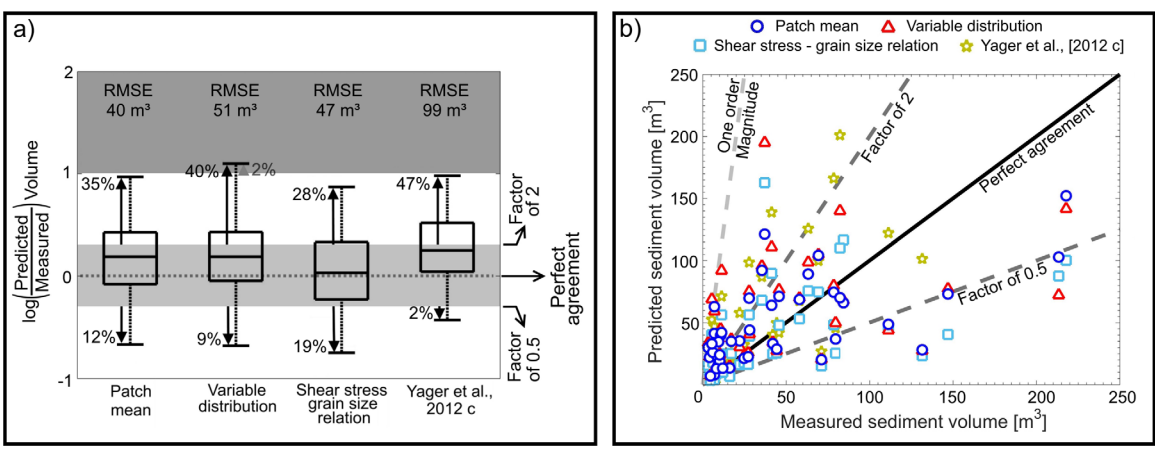

Figure 7. (a) The log of the ratio of the predicted to measured sediment volumes. Predicted bed load volumes by the Patch mean, Variable distribution and shear stress - grain size relation are compared to those of *Yager et al.* [2012c]. In the Figure Shear stress-grain size relation is our $\bar{\tau}_j - \bar{\tau} - D_{50j}$ relation, see text for other definitions. The line of perfect agreement denotes the measured volume was predicted exactly. The top and bottom of each box are the 25th and 75th percentiles and the middle line inside the box is the median value. Lines extending out of the box correspond to the maximum and minimum predicted volume ratios. Arrows and corresponding text denote the percent of the sediment volume predictions that are greater or less than a factor of 2 (black) and greater than a factor of 10 (grey). The light gray shaded area represents predictions within a factor of 2 of the measured values. The dark grey shaded area represent over predictions by more than an order magnitude. The volume at the top of each box corresponds to the RMSE of the predicted bed load volume. (b) Comparison of the measured and predicted sediment transport volumes for the same equations. Some predicted sediment volumes by *Yager et al.* [2012c] fall outside the box (6 sediment transport events, higher than 250 m^3).

Table 2. Prediction Errors in Sediment Flux Calculations[a]

	Patch Mean	Variable Distribution	Shear Stress Grain Size Relation	*Yager et al.* [2012c]
RMSE (m^3)	40	51	47	99
Within a factor of 2 (%)	53	51	53	51
Greater than 2 (%)	35	40	28	47
Less than 0.5 (%)	12	9	19	2
Overpredicted (%)	58	65	47	63
Underpredicted (%)	19	19	37	9

[a]"Within a factor of 2" denotes the percent of predicted sediment volumes that were within the range 0.5–2 of the measured values. "Greater than 2" and "Less than 0.5" denote the percent of predictions that were greater or less than a factor of 2, respectively. "Overpredicted" and "Underpredicted" denote predictions that were greater than 1.25 or lower than 0.75 times the measured transported volumes. We considered predictions within a ratio of 1 ± 0.25 as "successfully predicted." Shear stress – Grain size relation uses the $\bar{\tau}_j - \bar{\tau} - D_{50j}$ relations.

relations can be used to quantify shear stress variability between patch classes (Figure 8c). At low $\bar{\tau}$ (100 Pa) fine patches have applied shear stresses that are significantly lower than the reach averaged value. As $\bar{\tau}$ increases, $\bar{\tau}_j/\bar{\tau}$ approaches unity for most patch classes (500 Pa occurs at discharges of about 3.0 m^3/s in the Erlenbach), shear stress variability becomes relatively unimportant, and reach averaged shear stress may be adequate for sediment transport calculations.

We tested the $\bar{\tau}_j - \bar{\tau} - D_{50j}$ (using the $\bar{\tau}_{var\,D_{50}}$ version) relations in sediment transport calculations using the same measured sediment transport events from section 3.3. All the predicted volumes were of comparable magnitude with those calculated using the "Patch mean" method (Figure 7). The RMSE was 47 m^3, which is slightly higher than that from the "Patch mean" approach (40 m^3, Table 2) and less than half of that from *Yager et al.* [2012c] (99 m^3). 53% of the predictions were within a factor of two. The results obtained using the $\bar{\tau}_j - \bar{\tau} - D_{50j}$ relations suggests that they are well suited for bed load predictions.

4. Discussion

4.1. Predictions of Boundary Shear Stress and Sediment Transport Equations

We demonstrated that bed load transport estimations can be improved, compared to those that use reach averaged properties, when local characteristics of the flow and the spatial distribution of grain sizes are considered. We presented three different approaches for spatially distributed shear stresses: i) "Patch mean"; ii)

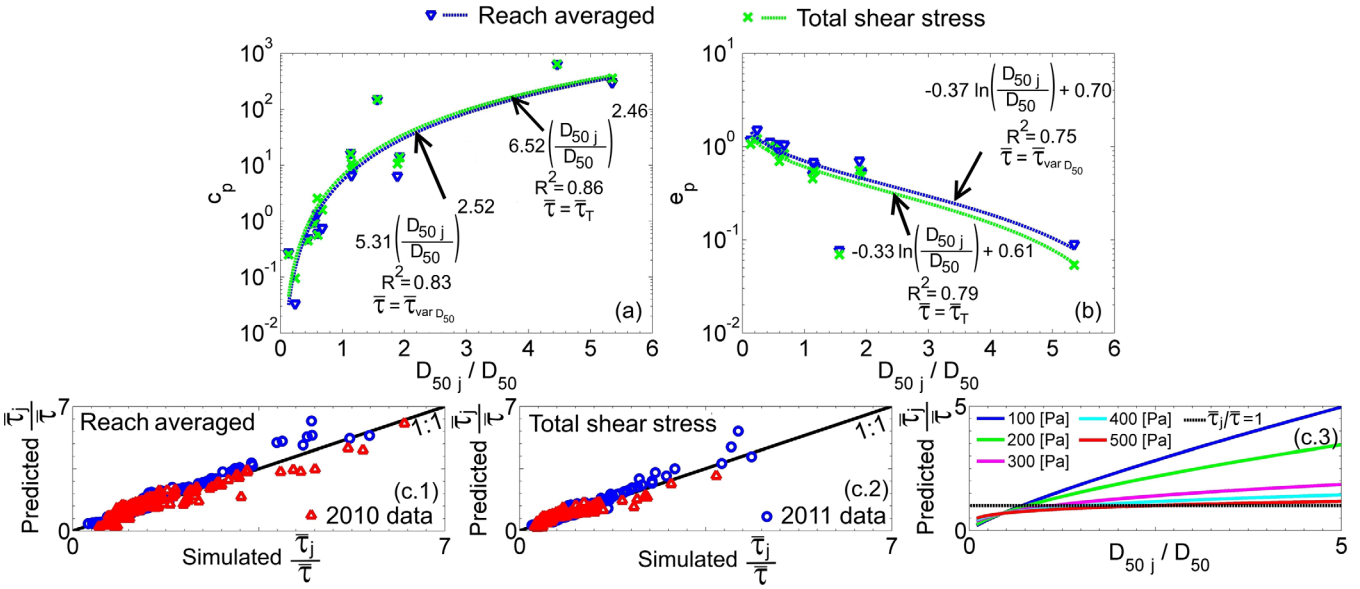

Figure 8. (a) Relations for the coefficient and (b) exponent of equation (17) as functions of the normalized patch class median grain size. (c.1 and c.2) A comparison of the hydrodynamic model's prediction the for patch class shear stress ratio ($\bar{\tau}_j/\bar{\tau}$) and those predicted by equations (18) and (19). (c.3) The predicted $\bar{\tau}_j/\bar{\tau}$ ratio as a function of the relative patch class grain size for a range of shear stresses. Continuous black lines in Figures 8c.1 and 8c.2 represents a 1:1 relation.

Table 3. Prediction Errors for Sediment Flux Calculations Using the Shear-Stress Grain Size Relation and 2004 Sediment Transport Data[a]

	2010	2011	*Egashira and Ashida* [1991]	*Rickenmann and Recking* [2011]	*Yager et al.* [2012b] Total	*Yager et al.* [2012c]
RMSE (m^3)	33	40	36	40	52	42
Within a factor of 2 (%)	27	53	20	53	60	27
Greater than 2 (%)	33	40	20	40	40	47
Less than 0.5 (%)	40	7	60	7	0	27
Overpredicted (%)	33	40	33	40	53	47
Underpredicted (%)	40	27	60	27	7	27

[a]See Table 2 for definitions. Each method is defined in the text. *Yager et al.* [2012c] use their full equations whereas all other methods are just different ways to calculate the reach-averaged shear stress for use in our $\bar{\tau}_j - \bar{\tau} - D_{50j}$ relations and sediment transport equations.

"Variable distribution"; and iii) $\bar{\tau}_j - \bar{\tau} - D_{50j}$ relations. For the "Variable distribution" approach we found that no single probability distribution was able to represent the observed spatially distributed shear stresses in each patch and simulated discharge with statistical confidence (see supporting information section S4). This approach predicted the most sediment transport events outside a factor of 2 of the measured volumes because it uses the full range of shear stresses applied on each patch class and all locally high and low values are included (Figure 7). Locally high shear stresses normally are accompanied by scour and filling, which are not included in our calculations. It is not the objective of this study to test the accuracy of each probability distribution used in the "Variable distribution" approach.

The "Patch mean" approach was more accurate than the original method of *Yager et al.* [2012c] in terms of sediment volume RMSE (m^3) and reducing systematic over-prediction but generally had a similar percentage of events within a factor of two of the measured values. The "Patch mean" and "Variable distribution" did not dramatically improve bedload estimates over the method of *Yager et al.* [2012c]. It is important, therefore, to consider that the accuracy achieved with these new methods must be contrasted with the field measurements and the numerical modeling efforts, which can be an obstacle for some practical applications. The *Yager et al.* [2012c] equation likely worked well because it predicts the mean shear stress fairly accurately for most of the sediment transporting flows (Figure 6a). This mean shear stress could have worked well because the shear stresses on each patch class approach the reach-averaged stress with increasing discharge (Figure 8c.3). However, if we had tested the *Yager et al.* [2012c] equation for a wider range of discharges, it is likely that its performance compared to our equation would decline because it systematically over-predicts $\bar{\tau}_m^*$ at higher discharges. A variable drag coefficient of the mobile sediment (C_m), instead of a constant one as assumed by *Yager et al.* [2012b], could result in a lower $\bar{\tau}_m^*$ at high discharge. The $\bar{\tau}_j - \bar{\tau} - D_{50j}$ relations are easier and more broadly applicable than the "Patch mean" and "Variable distribution" methods and can be used where data collection and/or numerical modeling are difficult to perform. The advantage of these equations is that they preserve the simplicity of reach-averaged relations while maintaining the accuracy of the spatially variable method (Figure 7). Only areas relevant for sediment transport, defined as $\tau_j^* \geq \tau_c^*$, were considered in our $\bar{\tau}_j - \bar{\tau} - D_{50j}$ relations, similar relations and bedload prediction accuracies were obtained when the whole wetted area was considered (see supporting information for further details).

4.2. Shear Stress Variations With Median Grain Size

Local shear stress has previosly been poorly correlated with local median grain size [*Lisle et al.*, 2000; *Nelson et al.*, 2010] and in our case it was also poorly correlated with patch class median grain size (section 3.2, Figure 5a). However, the mean patch class shear stress varied directly with patch class median grain size and scaled fairly well with the reach-averaged shear stress (Figures 5b, 8a, and 8b). This implies that sediment patches may not only be a response to shear stress divergences [*Nelson et al.*, 2010] but also to local stress magnitudes. Such a result is important for predicting the location and stability of sediment patches. In the particular case of salmon spawning, the ideal location for placement of relatively stable gravel could be potentially estimated from a shear stress map.

4.3. Relative Importance of Spatial Distribution of Shear Stresses and Grain Size

It is challenging to establish whether grain size or shear stress variations are more important in bedload predictions because of the nonlinear processes that govern sediment transport [*Recking*, 2013]. Flume

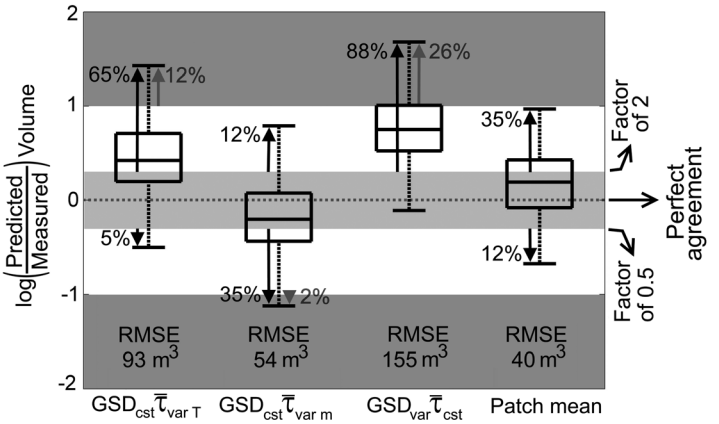

Figure 9. The log of the ratio of the predicted to measured sediment volumes when either the GSD or the distribution of shear stress was held constant (see text for definitions). The patch mean approach (see section 3.3) is included for comparison. See Figure 7 for an explanation of other figure properties.

experiments have shown that variations in local shear stress are relatively more important than those in grain size for bar formation [*Nelson et al.*, 2010]. In steep streams, field observations suggest that local flow, and not spatial grain size variations, is the primary driver of local bed load transport variability [*Yager et al.*, 2012a]. However, local grain-induced roughness may influence the initiation of sediment motion and therefore grain size variations could be important [*Scheingross et al.*, 2013].

To analyze whether a spatial distribution of shear stresses or grain sizes is more important we considered three cases: 1) for case $GSD_{cst}\,\bar{\tau}_{var\,T}$, we used each patch class averaged shear stress ("Patch mean" method of section 2.4) and assumed that the GSD for all patches was the reach-averaged value. Note that although all patches classes had the same GSD they had different shear stresses applied over different bed areas. 2) Case $GSD_{cst}\,\bar{\tau}_{var\,m}$ is the same except the mobile bed GSD was used (i.e., immobile grains were excluded), which may be more appropriate for bed load transport calculations. 3) In case $GSD_{var}\,\bar{\tau}_{cst}$, the shear stress acting on each patch class was the same for a given discharge and equal to that of the reach-averaged shear stress. The GSD was spatially variable and each patch class used its original measured grain sizes.

Sediment transport volumes in all three cases were less accurate than our "Patch mean" method (Figure 9) but were more accurate for the $GSD_{cst}\,\bar{\tau}_{var}$ cases than the $GSD_{var}\,\bar{\tau}_{cst}$ scenario. This suggests that the spatial variability of shear stress is relatively more important for sediment flux predictions than the spatial distribution of grain sizes, which has been also confirmed by the field study of *Segura and Pitlick* [2015]. The results of this experiment would need to be confirmed with sediment fluxes data from other streams but could help to decide how to allocate efforts to maximize sediment transport prediction accuracy with time or economic constrains.

4.4. Individual Contributions of Patch Classes to Sediment Fluxes

While some studies have found that, during low to moderate flow events, relatively fine patches are the only sources of bed sediment [*Garcia et al.*, 1999; *Vericat et al.*, 2008], others have observed motion on all patches [*Dietrich et al.*, 2005; *Yuill et al.*, 2010; *Yager et al.*, 2012a]. In our study, for a given discharge, the individual contributions of each patch class to the total transported volume depended on the patch's GSD, area (Figure 10) and applied stress. In general, patches with $D_{50j} < D_{50}$ contributed at least 80% of the total transported sediment volume. B, gbC and cgB patches in the 2010 data set and B and bgC patches in the 2011 data set had the lowest contribution (Figures 10a and 10b). Even during low to moderate flow events coarse patches ($D_{50j} > D_{50}$), whose contribution to the total transported volume was very small (Figures 10a and 10b), were still active and had some grain sizes in motion (Figures 10c and 10d).

In both data sets there were no patch classes that consistently contributed the largest fraction of the total transported volume. The contribution of each patch class to the total transported volume class was controlled by local topography, patch area and GSD. The topography determines flow routing throughout the channel, which directly affected the active area and applied shear stresses on each patch class. Patch class GSD influenced the relative mobility of different grain sizes and relative patch class area partly determines the proportional contribution of a patch class to the total sediment flux. The variability of different patch class contributions suggests that all patch classes must be considered in sediment flux predictions.

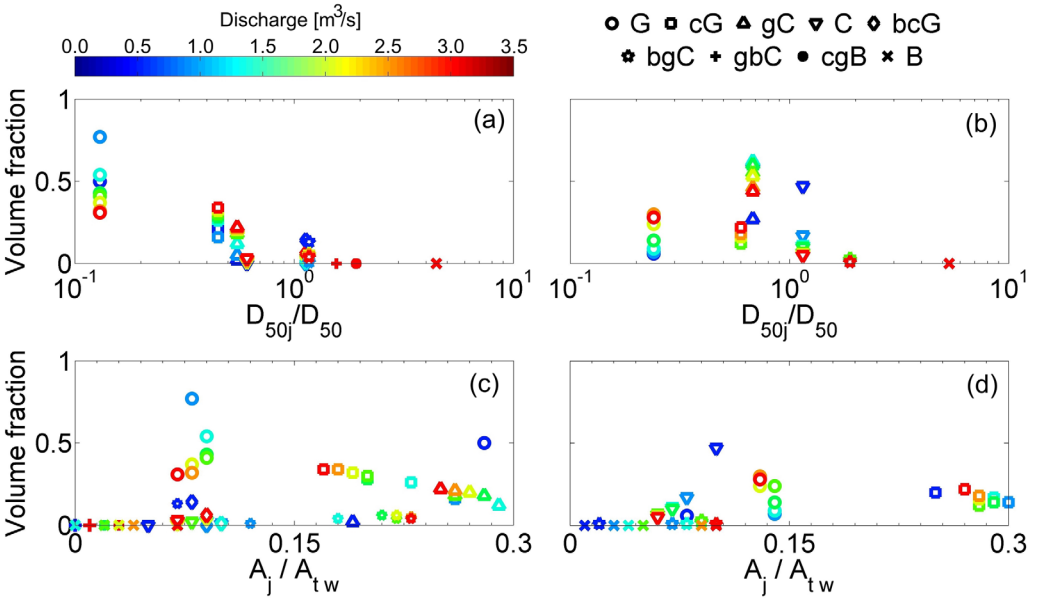

Figure 10. The volume fraction that each patch class contributes to the total transported volume as functions of (a, b) the normalized patch median grain size and (c, d) the relative area that each patch class occupied at each discharge. 2010 data are shown in Figures 10a and 10c, and 2011 are shown in Figures 10b and 10d.

4.5. Transferability of the Grain Size and Shear Stress Relation

To study the potential transferability of the $\bar{\tau}_j - \bar{\tau} - D_{50j}$ relation we used the published data of *Yager et al.* [2012a, 2012b] during 2004, which includes areas, GSD for each patch class, and channel characteristics used to calculate reach average shear stresses. The data were assumed to be valid during 2002–2006 when a total of 15 sediment transport events occurred. The extreme event of 2007 completely reorganized boulder steps [*Molnar et al.*, 2010] and all of the mobile patches, and therefore, we treat these data as if they were coming from a different stream to test the broader applicability of our equations. We used five different approaches using the 2004 data to estimate reach-averaged shear stress ($\bar{\tau}$) for use in our relation. Three approaches use the total shear stress ($\bar{\tau}_T$), which is easy to calculate in rivers where no detailed information is available. (1) For a given discharge we assumed that the reach-averaged shear stress was the same as what we calculated using the 2010 data and was equal to $\bar{\tau}^*_{var\,D_{50}}$ (see section 3.2). (2) We do the same thing as in (1) but with the 2011 data. Then, for the other three approaches we used the total shear stress calculated using the equations (3) [*Egashira and Ashida*, 1991], (4) [*Rickenmann and Recking*, 2011], and (5) [*Yager et al.*, 2012b]. Approaches (1) and (2) use equations (18a) and (19a) (Figures 8a and 8b), while approaches (3) to (5) use equations (18b) and (19b) to estimate the patch average shear stress. Note that we are not directly using the total shear stress for bed load transport predictions, we only use it to determine the shear stress on each patch class. Values used for sediment transport predictions in approaches (3) to (5) are summarized in supporting information Table S3. Details of the equations of *Egashira and Ashida* [1991] and *Rickenmann and Recking* [2011] can be found in the original publications and also in *Nitsche et al.* [2011]. For comparison purposes we include the original sediment volumes predicted by *Yager et al.* [2012c] for this time period.

The predicted sediment volumes from all approaches had similar RMSE, ranging from 33 to 52 m^3 (Figure 11, Table 3) and differences were largely caused by how the reach-averaged shear stress was specified. Predictions using the total shear stress (approaches 3–5), were roughly as accurate as those using the reach-averaged stress from the hydrodynamic model (approaches 1–2). Although the total shear stress does not include the effects of large roughness elements our relations for individual patch classes do.

The 2010, 2011, and *Egashira and Ashida* [1991] methods predicted sediment volumes that were within one order magnitude of the measured values. Most approaches using our sediment transport equation had a lower RMSE and more events predicted within a factor of two than those predicted by *Yager et al.* [2012c], which does not include the effects of patches. This improvement suggests that our method could be

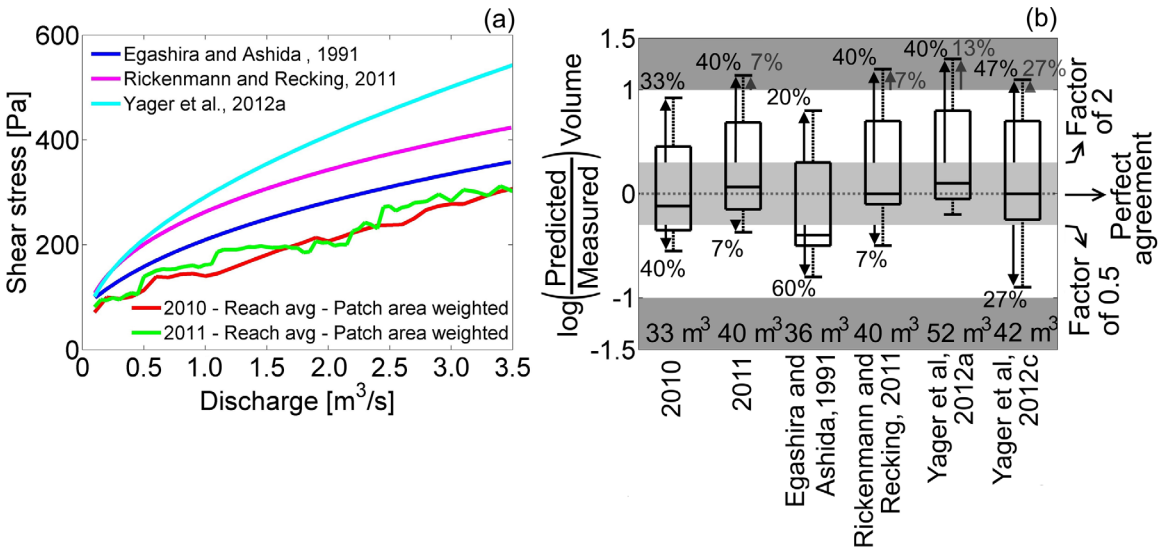

Figure 11. (a) Reach-averaged shear stress as a function of discharge. The shear stress for 2010 and 2011 used the $\tau_{var\,D_{50}}$ method, the total shear stress was calculated using resistance equations of *Egashira and Ashida* [1991], *Rickenmann and Recking* [2011], and *Yager et al.* [2012b]. (b) The log of the ratio of the predicted to measured sediment volume for sediment transport events during 2002–2006 at the Erlenbach. The results of *Yager et al.* [2012c] were included only as a reference and the volumes predicted in the original study are shown here. All other predictions used our $\tau_j - \tau - D_{50j}$ relations and sediment transport equation. See Figure 7 for an explanation of other figure properties.

capable of predicting fluxes of better accuracy than other methods available, but we would recommend using this method with caution until it has been further tested.

5. Conclusions

Including the spatial variability of flow and GSD in sediment transport calculations improved predictions compared to equations that only used reach-averaged properties. Nonetheless, achieving this increase in accuracy requires intense numerical modeling and detailed field measurements that can limit its applicability in practical cases. However, predictions were improved mainly because patch class shear stress directly correlated with patch class median grain size, which allowed for a better representation of local sediment mobility and hiding effects. Simple empirical relations of reach and patch class averaged shear stress with median grain size were developed and tested with our sediment transport equation. When using these relations the simplicity of reach averaged equations is preserved while the accuracy of including spatial variability is achieved. The relation between shear stress and surface median grain size is also a first step toward a theory to explain and predict the formation and location of sediment patches. It indicates that, at the patch scale, surface grain size and shear stress are coupled and the patch characteristics may not just be controlled by the divergence of shear stress. For accurate sediment transport predictions all patch classes must be considered; no particular patch class was consistently the greatest contributor to the total transported sediment volume. Individual contributions of each patch class depended on both GSD and area occupied. Finally, the spatial variability in the flow was relatively more important for accurate sediment fluxes than the spatial variability of the GSD.

Acknowledgments
Funding for this research was provided by an NSF Career award to E.M. Yager (0847799), the Chilean Government - CONICYT "Becas de Doctorado en el Extranjero – Becas Chile", and the Swiss Federal Research Institute WSL. Invaluable field assistance was provided by Heidi Smith, Alex Beer, and Manuel Nitsche. We thank Thomas Lisle, Catalina Segura and one anonymous reviewer for their constructive comments that helped to improve an earlier version of this manuscript. Please contact the corresponding author (mons0853@vandals.uidaho.edu) if you are interested in the topographic, sediment grain size distributions or hydraulic data. If you are interested in the Swiss bed load data please contact Dieter Rickenmann (dieter.rickenmann@wsl.ch).

References

Aziz, N. M., and D. E. Scott (1989), Experiments on sediment transport in shallow flows in high gradient channels, *Hydrol. Sci. J.*, *34*(4), 465–478, doi:10.1080/02626668909491352.

Barton, G. J., R. R. McDonald, J. M. Nelson, and R. R. Dinehart (2005), Simulation of flow and sediment mobility using a multidimensional flow model for the white sturgeon critical-habitat reach, 54 pp., *U.S. Geological Survey Scientific Investigations Report 2005-5230*, Kootenai River near Bonners Ferry, Idaho.

Bathurst, J. C., W. H. Graf, and H. H. Cao (1987), Bed load discharge equations for steep mountain rivers, in *Sediment Transport in Gravel Bed Rivers*, edited by C. R. Thorne, J. C. Bathurst, and R. D. Hey, pp. 453–477, John Wiley, Chichester, U. K.

Beer, A. R., J. M. Turowski, B. Fritschi, and D. H. Rieke-Zapp (2015), Field instrumentation for high-resolution parallel monitoring of bedrock erosion and bedload transport, *Earth Surf. Processes Landforms*, *40*(4), 530–541, doi:10.1002/esp.3652.

Bertoldi, W., P. Ashmore, and M. Tubino (2009), A method for estimating the mean bed load flux in braided rivers, *Geomorphology*, *103*, 330–340, doi:10.1016/j.geomorph.2008.06.014.

Bridge, J. S., and S. J. Bennett (1992), A model for entrainment and transport of sediment grain of mixed sizes, shapes, and densities, *Water Resour. Res.*, *28*(2), 337–363.
Buffington, J. M., and D. R. Montgomery (1997), A systematic analysis of eight decades of incipient motion studies, with special reference to gravel-bedded rivers, *Water Resour. Res.*, *33*(8), 1993–2029, doi:10.1029/97WR03138.
Buffington, J. M., and D. R. Montgomery (1999a), A procedure for classifying textural facies in gravel-bed rivers, *Water Resour. Res.*, *35*(6), 1903–1914, doi:10.1029/1999WR900041.
Buffington, J. M., and D. R. Montgomery (1999b), Effects of hydraulic roughness on surface textures of gravel-bedded rivers, *Water Resour. Res.*, *35*(11), 3507–3521.
Buxton, T. H., J. M. Buffington, D. Tonina, A. K. Fremier, and E. M. Yager (2015a), Modeling the Influence of Salmon Spawning on Hyporheic Exchange of Marine-Derived Nutrients in Gravel Stream beds, *Can. J. Fish. Aquat. Sci.*, *72*, 1146–1158, doi:10.1139/cjfas-2014-0413.
Buxton, T. H., J. M. Buffington, E. M. Yager, M. A. Hassan, and A. K. Fremier (2015b), The relative stability of salmon redds and unspawned streambeds, *Water Resour. Res.*, *51*, 6074–6092, doi:10.1002/2015WR016908.
Chen, L., and M. C. Stone (2008), Influence of bed material size heterogeneity on bedload transport uncertainty, *Water Resour. Res.*, *44*, W01405, doi:10.1029/2006WR005483.
Clayton, J. A., and J. Pitlick (2007), Spatial and temporal variations in bed load transport intensity in a gravel bed river bend, *Water Resour. Res.*, *43*, W02426, doi:10.1029/2006WR005253.
Comiti, F., and L. Mao (2012), Recent advances in the dynamics of steep channels, in *Gravel-Bed Rivers: Processes, Tools, Environments*, edited by M. Church, P. M. Biron, and A. G. Roy, pp. 351–377, John Wiley, Chichester, U. K.
Comiti, F., L. Mao, A. Wilcox, E. E. Wohl, and M. A. Lenzi (2007), Field-derived relationships for flow velocity and resistance in high-gradient streams, *J. Hydrol.*, *340*(1-2), 48–62, doi:10.1016/j.jhydrol.2007.03.021.
Conner, J. T., and D. Tonina (2014), Effect of cross-section interpolated bathymetry on 2D hydrodynamic model results in a large river, *Earth Surf. Processes Landforms*, *39*, 463–475, doi:10.1002/esp.3458.
Dietrich, W. E., and P. Whiting (1989), Boundary shear stress and sediment transport In river meanders of sand and gravel, in *River Meandering, Water Resour. Monogr.*, vol. 12, edited by S. Ikeda and G. Parker, pp. 1–50, AGU, Washington, D. C.
Dietrich, W. E., J. W. Kirchner, H. Ikeda, and F. Iseya (1989), Sediment supply and the development of the coarse surface layer in gravel-bedded rivers, *Nature*, *340*, 215–217, doi:10.1038/340215a0.
Dietrich, W. E., P. a. Nelson, E. Yager, J. G. Venditti, M. P. Lamb, and L. Collins (2005), Sediment patches, sediment supply, and channel morphology, in *4th IAHR Symposium on River, Coastal and Estuarine*., edited by G. Parker and M. H. Garcia, pp. 79–90, Taylor and Francis, Urbana, Ill.
Egashira, S., and K. Ashida (1991), Flow resistance and sediment transportation in streams with step-pool bed morphology, in *Fluvial Hydraulics of Mountain Regions*, edited by A. Armanini and G. Di Silvio, pp. 45–58, Springer, Berlin.
Einstein, H. A. (1950), The bed-load function for sediment transportation in open channel flows, *Soil Conserv. Serv.*, (1026), 1–31.
Ferguson, R. (2007), Flow resistance equations for gravel- and boulder-bed streams, *Water Resour. Res.*, *43*, W05427, doi:10.1029/2006WR005422.
Ferguson, R. I. (2003), The missing dimension: Effects of lateral variation on 1-D calculations of fluvial bedload transport, *Geomorphology*, *56*, 1–14, doi:10.1016/S0169-555X(03)00042-4.
Garcia, C., J. B. Laronne, and M. Sala (1999), Variable source areas of bedload in a gravel-bed stream, *J. Sediment. Res.*, *69*(1), 27–31, doi:10.2110/jsr.69.27.
Ghilardi, T., M. J. Franca, and a J. Schleiss (2014), Bulk velocity measurements by video analysis of dye tracer in a macro-rough channel, *Meas. Sci. Technol.*, *25*(3), 035003, doi:10.1088/0957-0233/25/3/035003.
Graf, W. H., and L. Suszka (1987), Sediment transport in steep channels, *J. Hydrosci. Hydraul. Eng.*, *5*, 11–26.
Hajimirzaie, S. M., A. G. Tsakiris, J. H. J. Buchholz, and A. N. Papanicolaou (2014), Flow characteristics around a wall-mounted spherical obstacle in a thin boundary layer, *Exp. Fluids*, *55*(6), 1–14, doi:10.1007/s00348-014-1762-0.
Hassan, M. A., D. Tonina, and T. H. Buxton (2015), Does small-bodied salmon spawning activity enhance streambed mobility?, *Water Resour. Res.*, *51*, 7467–7484, doi:10.1002/2015WR017079.
Jarrett, R. D. (1984), Hydraulics of high-gradient streams, *J. Hydraul. Eng.*, *110*(11), 1519–1539.
Kinzel, P. J., J. M. Nelson, and A. K. Heckman (2009), Response of sandhill crane (Grus canadensis) riverine roosting habitat to changes in stage and sandbar morphology, *River Res. Appl.*, *25*(2), 135–152, doi:10.1002/rra.1103.
Kleinhans, M. G., and L. C. van Rijn (2002), Stochastic Prediction of Sediment Transport in Sand-Gravel Bed Rivers, *J. Hydraul. Eng.*, *128*(4), 412–425, doi:10.1061/?ASCE?0733-9429?2002?128:4?412?CE.
Kondolf, G. M., and M. G. Wolman (1993), The sizes of salmonid spawning gravels, *Water Resour. Res.*, *29*(7), 2275–2285, doi:10.1029/93WR00402.
Lacey, R. W. J. W. J., and A. G. Roy (2008), The spatial characterization of turbulence around large roughness elements in a gravel-bed river, *Geomorphology*, *102*(3-4), 542–553, doi:10.1016/j.geomorph.2008.05.045.
Laronne, J. B., C. García, and I. Reid (2000), Mobility of patch sediment in gravel bed streams: Patch character and its implications for bedload, in *Gravel-Bed Rivers V*, edited by M. P. Mosley, pp. 249–289, N. Z. Hydrol. Soc. Inc., Wellington.
Lenzi, M. A., and V. D'agostino (1999), Bedload transport in the instrumented catchment of the Rio Cordon Part II: Analysis of the bedload rate, *Catena*, *36*, 191–204.
Lenzi, M. A., V. D'Agostino, and P. Billi (1999), Bedload transport in the instrumented catchment of the Rio Cordon PArt I: Analysis of bedload records, conditions and threshold of bedload entrainment, *Catena*, *36*, 171–190, doi:10.1016/S0341-8162(99)00017-X.
Lisle, I. G., C. W. Rose, W. L. Hogarth, P. B. Hairsine, G. C. Sander, and J.-Y. Parlange (1998), Stochastic sediment transport in soil erosion, *J. Hydrol.*, *204*, 217–230, doi:10.1016/S0022-1694(97)00123-6.
Lisle, T. E., H. Ikeda, and F. Iseya (1991), Formation of stationary alternate bars in a steep channel with mixed-size sediment: A flume experiment, *Earth Surf. Processes Landforms*, *16*(5), 463–469, doi:10.1002/esp.3290160507.
Lisle, T. E., F. Iseya, and H. Ikeda (1993), Response of a channel with alternate bars to a decrease in supply of mixed-size bed load: A flume experiment, *Water Resour. Res.*, *29*(11), 3623–3629, doi:10.1029/93WR01673.
Lisle, T. E., J. M. Nelson, J. Pitlick, M. A. Madej, and B. L. Barkett (2000), Variability of bed mobility in natural, gravel-bed channels and adjustments to sediment load at local and reach scales, *Water Resour. Res.*, *36*(12), 3743–3755, doi:10.1029/2000WR900238.
Maturana, O., D. Tonina, J. A. McKean, J. M. Buffington, C. H. Luce, and D. Caamaño (2014), Modeling the effects of pulsed versus chronic sand inputs on salmonid spawning habitat in a low-gradient gravel-bed river, *Earth Surf. Processes Landforms*, *39*, 877–889, doi:10.1002/esp.3491.

Mcdonald, R. R., J. M. Nelson, and J. P. Bennett (2005), Multi-dimensional surface water modeling system user's guide, *US Geological Survey Techniques in Water Resources Investigations 11-B2*, 136 pp. [Available at http://wwwbrr.cr.usgs.gov/projects/GEOMORPH_Lab/WebHelp_Pro/MD_SWMS.htm.]

Miller, A. J., and B. L. Cluer (1998), Modeling considerations for simulation of flow in bedrock channels, in bedrock channels, in *Rivers Over Rock: Fluvial Processes in Bedrock Channels*, edited by K. J. Tinkler and E. E. Wohl, AGU, Washington, D. C.

Molnar, P., A. L. Densmore, B. W. McArdell, J. M. Turowski, and P. Burlando (2010), Analysis of changes in the step-pool morphology and channel profile of a steep mountain stream following a large flood, *Geomorphology*, *124*(1-2), 85–94, doi:10.1016/j.geomorph.2010.08.014.

Mueller, E., R. Batalla, C. Garcia, and A. Bronstert (2008), Modeling bed-load rates from fine grain-size patches during small floods in a gravel-bed river, *J. Hydraul. Eng.*, *134*(10), 1430–1439, doi:10.1061/(ASCE)0733-9429(2008)134:10(1430).

Mueller, E. R., and J. Pitlick (2014), Sediment supply and channel morphology in mountain river systems: 2. Single thread to braided transitions, *J. Geophys. Res. Earth Surf.*, *119*, 1516–1541, doi:10.1002/2013JF002843.

Nelson, J. M., and R. R. McDonald (1995), *Mechanics and Modeling of Flow and Bed Evolution in Lateral Separation Eddies*, US Geological Survey GRand Canyon Monitoring and Research Center, Flagstaff, Ariz.

Nelson, J. M., and J. D. Smith (1989), Evolution and stability of erodible channel beds, in *River Meandering, Water Resour. Monogr.*, edited by S. Ikeda and G. Parker, AGU, Washington, D. C.

Nelson, J. M., J. P. Bennett, and S. M. Wiele (2003), Flow and Sediment-Transport Modeling, in *Tools in Fluvial Geomorphology*, edited by G. M. Kondolf and H. Piégay, John Wiley & Sons, Ltd., Chichester, U. K., doi:10.1002/0470868333.ch18.

Nelson, P. A., J. G. Venditti, W. E. Dietrich, J. W. Kirchner, H. Ikeda, F. Iseya, and L. S. Sklar (2009), Response of bed surface patchiness to reductions in sediment supply, *J. Geophys. Res.*, *114*, F02005, doi:10.1029/2008JF001144.

Nelson, P. A., W. E. Dietrich, and J. G. Venditti (2010), Bed topography and the development of forced bed surface patches, *J. Geophys. Res.*, *115*, F04024, doi:10.1029/2010JF001747.

Nelson, P. A., D. Bellugi, and W. E. Dietrich (2014), Delineation of river bed-surface patches by clustering high-resolution spatial grain size data, *Geomorphology*, *205*, 102–119, doi:10.1016/j.geomorph.2012.06.008.

Nicholas, A. P. (2000), Modelling bedload yield braided gravel bed rivers, *Geomorphology*, *36*, 89–106, doi:10.1016/S0169-555X(00)00050-7.

Nitsche, M., D. Rickenmann, J. M. Turowski, A. Badoux, and J. W. Kirchner (2011), Evaluation of bedload transport predictions using flow resistance equations to account for macro-roughness in steep mountain streams, *Water Resour. Res.*, *47*, W08513, doi:10.1029/2011WR010645.

Pagliara, S., and P. Chiavaccini (2006), Flow resistance of rock chutes with protruding boulders, *J. Hydraul. Eng.*, *132*(6), 545–552, doi:10.1061/(ASCE)0733-9429(2006)132:6(545).

Paintal, A. S. (1971), A stochastic model of bed load transport, *J. Hydraul. Res.*, *9*(4), 527–554, doi:10.1080/00221687109500371.

Paola, C. (1996), Incoherent structure: Turbulence as a metaphor for stream braiding, in *Coherent Flow Structures in Open Channels*, edited by P. Ashworth et al., pp. 706–723, John Wiley, Chichester, U. K.

Paola, C., and R. Seal (1995), Grain size patchiness as a cause of selective deposition and downstream fining, *Water Resour. Res.*, *31*(5), 1395–1407.

Papanicolaou, A. N., and C. Kramer (2005), The role of relative submergence on cluster microtopography and bedload predictions in mountain streams, in *Proceeding of the 4th IAHR Conference on River, Coastal and Estuarine Morphodynamics*, edited by G. Parker and M. H. Garcia, pp. 1083–1086, Taylor and Francis, Urbana, Ill.

Parker, G. (1990), Surface-based bedload transport relation for gravel rivers, *J. Hydraul. Res.*, *28*(4), 417–436, doi:10.1080/00221689009499058.

Parker, G., C. Paola, and S. Leclair (2000), Probabilistic exner sediment continuity equation for mixtures with no active layer, *J. Hydraul. Eng.*, *126*(11), 818–826, doi:10.1061/(ASCE)0733-9429(2000)126:11(818).

Pasternack, G. B., A. T. Gilbert, J. M. Wheaton, and E. M. Buckland (2006), Error propagation for velocity and shear stress prediction using 2D models for environmental management, *J. Hydrol.*, *328*(1-2), 227–241, doi:10.1016/j.jhydrol.2005.12.003.

Rattray, M. J., and E. Mitsuda (1974), Theoretical analysis of conditions in a salt wedge, *Estuarine Coastal Mar. Sci.*, *2*, 375–394.

Recking, A. (2013), An analysis of nonlinearity effects on bed load transport prediction, *J. Geophys. Res. Earth Surf.*, *118*, 1264–1281, doi:10.1002/jgrf.20090.

Rickenmann, D. (1997), Sediment transport in Swiss torrents, *Earth Surf. Processes Landforms*, *22*(10), 937–951, doi:10.1002/(SICI)1096-9837(199710)22:10<937::AID-ESP786>3.0.CO;2-R.

Rickenmann, D. (2001), Comparison of bed load transport in torrents and gravel bed streams, *Water Resour. Res.*, *37*(12), 3295–3305, doi:10.1029/2001WR000319.

Rickenmann, D. (2005), Geschiebetransport bei steilen Gefällen, in *Mitteilungen der Versuchsanstalt für Wasserbau*, Hydrologie und Glaziologie, ETH Zurich, Nr. 190, pp. 107–119.

Rickenmann, D., and B. W. McArdell (2007), Continuous measurement of sediment transport in the Erlenbach stream using piezoelectric bedload impact sensors, *Earth Surf. Processes Landforms*, *32*(9), 1362–1378, doi:10.1002/esp.1478.

Rickenmann, D., and A. Recking (2011), Evaluation of flow resistance in gravel-bed rivers through a large field data set, *Water Resour. Res.*, *47*, W07538, doi:10.1029/2010WR009793.

Rickenmann, D., J. M. Turowski, B. Fritschi, A. Klaiber, and A. Ludwig (2012), Bedload transport measurements at the Erlenbach stream with geophones and automated basket samplers, *Earth Surf. Processes Landforms*, *37*(9), 1000–1011, doi:10.1002/esp.3225.

Scheingross, J. S., E. W. Winchell, M. P. Lamb, and W. E. Dietrich (2013), Influence of bed patchiness, slope, grain hiding, and form drag on gravel mobilization in very steep streams, *J. Geophys. Res. Earth Surf.*, *118*, 982–1001, doi:10.1002/jgrf.20067.

Schneider, J. M., D. Rickenmann, J. M. Turowski, K. Bunte, and J. W. Kirchner (2015), Applicability of bed load transport models for mixed-size sediments in steep streams considering macro-roughness, *Water Resour. Res.*, *51*, 5260–5283, doi:10.1002/2014WR016417.

Segura, C., and J. Pitlick (2015), Coupling fluvial-hydraulic models to predict gravel transport in spatially variable flows, *J. Geophys. Res. Earth Surf.*, *120*, 834–855, doi:10.1002/2014JF003302.

Shamloo, H., N. Rajaratnam, and C. Katopodis (2001), Hydraulics of simple habitat structures, *J. Hydraul. Res.*, *39*(4), 351–366.

Shvidchenko, A. B., and G. Pender (2000), Flume study of the effect of relative depth on the incipient motion of coarse uniform sediments, *Water Resour. Res.*, *36*(2), 619–628.

Smart, G. (1984), Sediment transport formula for steep channels, *J. Hydraul. Eng.*, *110*(3), 267–276, doi:10.1061/(ASCE)0733-9429(1984)110:3(267).

Strom, K. B., and A. N. Papanicolaou (2007), ADV measurements around a cluster microform in a shallow mountain stream, *J. Hydraul. Eng.*, *133*(12), 1379–1389, doi:10.1061/(ASCE)0733-9429(2007)133:12(1379).

Sun, Z., and J. Donahue (2000), Statistically derived bedload formula for any fraction of nonuniform sediment, *J. Hydraul. Eng.*, *126*(2), 105–111, doi:10.1061/(ASCE)0733-9429(2000)126:2(105).

Tritico, H. M., and R. H. Hotchkiss (2005), Unobstructed and obstructed turbulent flow in gravel bed rivers, *J. Hydraul. Eng.*, *131*(8), 635–645, doi:10.1061/(ASCE)0733-9429(2005)131:8(635).

Tsakiris, A. G., a. N. T. Papanicolaou, S. M. Hajimirzaie, and J. H. J. Buchholz (2014), Influence of collective boulder array on the surrounding time-averaged and turbulent flow fields, *J. Mt. Sci.*, *11*(6), 1420–1428, doi:10.1007/s11629-014-3055-8.

Turowski, J., and D. Rickenmann (2011), Measuring the statistics of bed-load transport using indirect sensors, *J. Hydraul. Eng.*, *137*(1), 116–121, doi:10.1061/(ASCE)HY.1943-7900.0000277.

Turowski, J. M., E. M. Yager, A. Badoux, D. Rickenmann, and P. Molnar (2009), The impact of exceptional events on erosion, bedload transport and channel stability in a step-pool channel, *Earth Surf. Processes Landforms*, *34*(12), 1661–1673, doi:10.1002/esp.1855.

Turowski, J. M., A. Badoux, J. Leuzinger, and R. Hegglin (2013), Large floods, alluvial overprint, and bedrock erosion, *Earth Surf. Processes Landforms*, *38*(9), 947–958, doi:10.1002/esp.3341.

Vericat, D., R. J. Batalla, and C. N. Gibbins (2008), Sediment entrainment and depletion from patches of fine material in a gravel-bed river, *Water Resour. Res.*, *44*, W11415, doi:10.1029/2008WR007028.

Whittaker, J. G. (1986), An equation for predicting bedload transport in steep mountain step-pool stream, in *9th Australasian Fluid Mechanics Conference*, pp. 358–361, Australasian Fluid Mechnics Society, Auckland, New Zealand.

Wu, F.-C., and K.-H. Yang (2004), A stochastic partial transport model for mixed-size sediment: Application to assessment of fractional mobility, *Water Resour. Res.*, *40*, W04501, doi:10.1029/2003WR002256.

Yager, E. M., J. W. Kirchner, and W. E. Dietrich (2007), Calculating bed load transport in steep boulder bed channels, *Water Resour. Res.*, *43*, W07418, doi:10.1029/2006WR005432.

Yager, E. M., W. E. Dietrich, J. W. Kirchner, and B. W. McArdell (2012a), Patch dynamics and stability in steep, rough streams, *J. Geophys. Res.*, *117*, F02010, doi:10.1029/2011JF002253.

Yager, E. M., W. E. Dietrich, J. W. Kirchner, and B. W. McArdell (2012b), Prediction of sediment transport in step-pool channels, *Water Resour. Res.*, *48*, W01541, doi:10.1029/2011WR010829.

Yager, E. M., J. M. Turowski, D. Rickenman, and B. W. McArdell (2012c), Sediment supply, grain protrusion, and bedload transport in mountain streams, *Geophys. Res. Lett.*, *39*, L10402, doi:10.1029/2012GL051654.

Yuill, B., M. Nichols, and E. Yager (2010), Coarse bed material patch evolution in low-order, ephemeral channels, *Catena*, *81*(2), 126–136, doi:10.1016/j.catena.2010.02.002.

Water Resources Research

Supporting Information for

A probabilistic formulation of bed load transport to include spatial variability of flow and surface grain size distributions

Angel Monsalve[1,2], Elowyn M. Yager[2], Jens M. Turowski[3], Dieter Rickenmann[4]

[1]Departamento de Ingeniería en Obras Civiles, Universidad de la Frontera, Francisco Salazar 1145, Temuco, Chile

[2]Civil Engineering, Center for Ecohydraulics Research, University of Idaho, 322 E. Front street, Boise, 83702, USA

[3]Helmholtz Centre Potsdam, GFZ German Research Centre for Geosciences, Telegrafenberg 14473 Potsdam, Germany

[4] Swiss Federal Research Institute WSL, Mountain Hydrology and Mass Movements, Zürcherstrasse 111, 8903 Birmensdorf, Switzerland

Contents of this file

Text S1 to S8
- Text S1: Flow modelling
- Text S2: Reach averaged velocity
- Text S3: Calibration of drag coefficient
- Text S4: Distribution of shear stress
- Text S5: Hiding functions
- Text S6: Limited Sediment Supply
- Text S7: Shear stress variations with median grain size for the whole wetted surface
- Text S8: Prediction and measurements uncertainties

Figures S1 to S3
- Figure S1: Comparison between spatially constant and variable drag coefficient
- Figure S2: The log of the ratio of the predicted to measured sediment volume for different hiding functions.
- Figure S3: Shear stress and sediment transport predictions using the whole wetted surface

Tables S1 to S3
- Table S1: Performance of different probability distributions
- Table S2: Hiding functions used in bed load calculations
- Table S3: Field measurements used to predict reach-averaged velocity and sediment transport

References

Introduction

A probabilistic bed load transport formulation that explicitly includes local variations in the flow field and grain size distribution was developed and tested at the Erlenbach, a 10% gradient stream in the Swiss Pre-Alps. Spatial variability of bed surface texture was included as patches of sediment. The average shear stress in each patch class was well correlated with the reach-averaged shear stress and the patch median surface grain size. An empirical relation was formulated between patch and reach-averaged shear stresses and grain sizes. When used in our bed load transport equation, this relation had a similar accuracy to that one that includes shear stress distributions on each patch and the simplicity of a reach-averaged approach. In this supporting material we provide details to support some of our assumptions in the probabilistic formulation development. We also analyze the sensitivity and uncertainties of the model.

Text S1: Flow modelling

We obtained our spatially variable flow field using a quasi-3D model, FaSTMECH, which solves the full vertically averaged and Reynolds-averaged momentum equations. Vertical velocity profiles are calculated along the streamlines of the vertically averaged flow, and secondary flow is calculated across those streamlines [*Nelson and Smith*, 1989]. Vertical accelerations, as well as aeration, can be very important in a step-pool river and the model probably does not fully capture the vertical flow complexity. We attempted to simultaneously measure water surface elevation and local velocity to use a fully 3D model, but high velocities, even for moderate discharges, made the measuring process extremely dangerous. The use of a full 3D model could produce more accurate estimates of boundary shear stress, but given the good agreement between the measured and predicted surface water elevations and average velocities, and the quality of the topography and bathymetry we used, we believe that the use of a quasi-3D model is be appropriate for our analysis.

Text S2: Reach averaged velocity

The reach averaged velocity (U) was calculated with

$$U = \sqrt{\frac{2gS\lambda_x h}{\frac{A_{IF}C_I}{w} + C_m\left(\lambda_x - \lambda_w\right)}}, \tag{S1}$$

where g is the acceleration due to gravity, S the average bed slope, λ_x the downstream spacing between steps, h the average flow depth, A_{IF} the bed-perpendicular area of immobile grains, w the channel width, C_I ($=157\left(h/p_u\right)^{-1.6}$) the drag coefficient for immobile grains with p_u the protrusion of the immobile steps, C_m ($=0.4$) the drag coefficient for mobile sediment, and λ_w the downstream step length. Equation (S1) must be solved iteratively until the predicted unit discharge ($q = Uh$) equals the measured one.

Text S3: Calibration of drag coefficients

We used a spatially constant drag coefficient, C_d, that inversely varied with discharge. This condition has been described by *Lisle et al.* [2000] as "equivalent to assuming that the flow responds extremely slowly to changes in roughness", meaning that roughness effects are averaged by the flow over spatial scales larger than that of the actual source of roughness. Although not for channels as steep as the Erlenbach, the studies of *Lisle et al.* [2000], *Nelson et al*. [2010] and *Segura and Pitlick* [2015] have shown that the use of constant drag coefficient results in similar local shear stress values compared to those determined using a variable drag coefficient. This is mainly because there is a trade-off between the local drag coefficient and velocity values. For example, if the grain size is included in the drag distribution patches of coarse grains will have a rougher surface than fine patches, consequently they will have a higher drag coefficient and the

velocity will decrease. The opposite will occur in fine patches, a lower drag coefficient associated with their finer grain size will result is higher velocities. This feedback ultimately results in similar local shear stress values (see discussion by [*Lisle et al.*, 2000]). As a first guess for C_d we used the relation of *Pasternack et al.* [2006] and assumed a Manning's roughness factor (n) of 0.1 (see equation 1.2 in the original study for more details). We then calibrated C_d by matching the water surface elevations predicted by the model to those obtained using the $h-Q$ rating curves and by matching the model-predicted reach-averaged velocity with the flow velocity obtained from the *Yager et al.* [2012] method. The selection of an initial n did not affect the final result, but did speed up the iteration process.

We tested if the distribution of dimensionless shear stresses in each patch class varied significantly when a spatially variable drag coefficient was considered instead of a spatially constant one. Our analysis considered only a set of representative discharges (Figure S1) from where we compared the dimensionless mean shear stress for each patch class (τ_j^*) and its standard deviation. For the spatially variable case the drag coefficient was calculated as a function of roughness height (z_0) using *Whiting and Dietrich*'s [1991] equation, where $z_0 = 0.1D_{84j}$ (with j the patch class and D_{84j} the 84th percentile of bed material grain size dsitribution). However, given our fine topography the geometry of the relatively coarse patches classes (bgC, gbC, cgB, and B) was captured and explicitly included in the numerical model, so using their respective D_{84j} would results in very large roughness heights relatively to the flow depth. Given that the spatial variation in topography of these relatively coarse patch classes was included in the mesh, we assumed that the D_{84j} of G patch class was a better representation to calculate z_0. Our results showed practically no variation in τ_j^* and its standard deviation due to the use of a variable drag coefficient compared to a constant one. These results are consistent

with those of *Lisle et al.* [2000] , *Nelson et al.* [2010] and *Segura and Pitlick* [2015] and supported our choice of using a constant drag coefficient for all our discharges.

Our simulations used a grid with a 10 cm node spacing, which is a fairly fine considering that the median grain size for the mobile fraction (D_{50m}) was between 5.8 - 7.4 cm for the 2010 and 2011 data sets, respectively. Given this spatial resolution, a major portion of the form drag was captured by the topography, while skin drag was accounted in the drag coefficient (C_d).The drag coefficient was a function of the grid size, and we analyzed the model sensitivity to this. We found that a 10 cm spacing gave the best balance between the RMSE of the water surface elevations (WSE) and modelling efforts. A 20 cm grid size required larger C_d values and the WSE RMSE was higher despite the model converging faster than when a 10 cm grid was used. A 5 cm grid size required slightly lower C_d values than a 10 cm grid size, but we had several problems reaching convergence, and in some cases we did not achieve it. For those simulations in which we successfully reached convergence, the WSE RMSE was not lower than that of a 10 cm grid size model but was more comparable to that of the 20 cm grid size.

Text S4: Distribution of shear stresses

Parameter estimation for shear stress distributions (See section 2.5 in the main text) was calculated using the maximum-likelihood estimation (MLE), where the objective is to find the model parameter values (θ) that maximize the likelihood function ($L(\theta) = \prod_{i=1}^{n} f(x_i \mid \theta)$, with x_i being the observed values) [*Fleiss et al.*, 2004]. One advantage of using the (MLE) is that is independent of the histogram bin size, which is required for example when the parameters are obtained via minimizing the χ^2 (see for example *Segura and Pitlick* [2015]). Notice that our calculations of χ^2 were not for parameter estimation but to test our null hypothesis (observed

shear stresses comes from the reference probability distribution). To calculate the χ^2 score, in particular to estimate the histogram bin width we used the Freedman-Diaconis rule. If a given bin had less than five observations, based on the number of wetted nodes and shear stresses range in each patch class and discharge, we pooled it with neighboring bins until the count in each bin was at least five. Our results showed that no single probability distribution was systematically able to represent the observed spatially distributed shear stresses in each patch class and simulated discharge range with statistically confidence (Table S1).

Text S5: Hiding functions

Our sediment transport equations are based on the work of *Parker* [1990] and *Yager et al* [2012a, 2012b]. The hiding function we used, "Erlenbach - Mobile", is the one proposed by *Yager et al.* [2012a] (Table S2), which is valid for the mobile sediment fraction and was developed using tracer particles in our study reach. To analyze the sensitivity of our predicted sediment volumes to the selected hiding function we calculated, using the Patch Mean method and a range of hiding functions, all the sediment transport events from the 2010 and 2011 data sets.

The dimensionless critical shear stress for the i^{th} grain size class at the j^{th} patch class is given by:

$$\tau^*_{ci\,j} = \alpha \left(\frac{D_{i\,j}}{D_{50}} \right)^{\beta}, \qquad \text{(S2)}$$

where α and β were varied (Table S2). The hiding functions were those by *Yager et al.* [2012a], the original *Parker* [1990] equation and one derived for the Rio Cordon [*Mao and Lenzi*, 2007], an alpine high-gradient, step–pool stream located in Italy.

Sediment volumes using the "Parker" hiding function *Parker* [1990] were almost always overpredicted by over an order magnitude and had the largest RMSE compared to the other hiding functions (Figure S2). The "Rio Cordon" hiding function predicted sediment transport volumes more accurately than "Parker", but tended to underpredict values. The most accurate results were obtained using the two hiding functions of *Yager et al.* [2012a], "Erlenbach Total" and "Erlenbach Mobile". The selection of an adequate hiding function is therefore crucial to obtain accurate sediment transport predictions. In rivers that do not have calibrated hiding functions, a sensitivity analysis of hiding functions is recommended.

Text S6: Limited sediment supply

The upstream sediment supply was included by scaling the predicted total transport rate by the volumetric proportion of the bed covered by relatively mobile sediment $\left(Am / A_T\right) Z_m^*$, where $Z_m^* = Z_t / Z_{t0}$ is the ratio of the thickness of the mobile sediment deposit at the time of an individual flow event (Z_t) to that immediately after the last extreme event (Z_{t0}). The percent step protrusion ($p_{u\%t}$) varies with time [*Yager et al.*, 2012b] and is related to the thickness of the mobile sediment deposit and the mean immobile grain diameter (D_I) through:

$$Z_t = D_I \left(1 - p_{u\%t}\right), \tag{S3}$$

and

$$p_{u\%t} = 0.15 t^{0.21}, \tag{S4}$$

where t is the time elapsed since the last extreme event (in units of months). Z_{t0} is calculated setting $t=1$ in equation (S4). Assuming D_I is constant during the period of analysis Z_m^* can be simplified as:

$$Z_m^* = \frac{Z_t}{Z_{t0}} = \frac{D_I\left(1-0.15t^{0.21}\right)}{D_I\left(1-0.15t^{0.21}\right)\Big|_{t=1}} = \frac{1}{0.85}\left(1-0.15t^{0.21}\right), \quad \text{(S5)}$$

Text S7: Shear stress variations with median grain size for the entire wetted surface

In our $\overline{\tau}_j - \overline{\tau} - D_{50j}$ relations we only considered areas where the local dimensionless shear stress was higher than the dimensionless critical shear stress ($\tau_j^* \geq \tau_c^*$). This eliminates a portion of the low shear stress values, especially for coarse patches (i.e. Boulder patches), and improves the correlation between patch mean shear stress and median grain size. If the whole wetted area is considered (i.e. without filtering those values below τ_c^*) the patch mean shear stress ($\overline{\tau}_j$) still increased with higher D_{50j} for all patch classes except for Boulder patches (Figure S3). Although Boulder patches did not follow the trend of the other patch classes, similar equations to the original $\overline{\tau}_j - \overline{\tau} - D_{50j}$ relations can be obtained and used for sediment transport calculations (Figure S3 b and c).

$$c_p = 0.98\left(\frac{D_{50j}}{D_{50}}\right)^{0.82} \quad , \overline{\tau} = \overline{\tau}_{var\ D_{50}} , R^2 = 0.44 \quad \text{(S6)}$$

$$c_p = 0.50\left(\frac{D_{50j}}{D_{50}}\right)^{0.93} \quad , \overline{\tau} = \overline{\tau}_T \quad , R^2 = 0.46 \quad \text{(S7)}$$

$$e_p = -0.14 \ln\left(\frac{D_{50j}}{D_{50}}\right) + 1.01 \qquad , \overline{\tau} = \overline{\tau}_{var\ D_{50}} , R^2 = 0.43 \tag{S8}$$

$$e_p = -0.14 \ln\left(\frac{D_{50j}}{D_{50}}\right) + 0.99 \qquad , \overline{\tau} = \overline{\tau}_T \qquad , R^2 = 0.44 \tag{S9}$$

We used the same test described in Section 3.3 to determine the accuracy of these relations when used in sediment transport equations. Equations (S6) to (S9) were almost as accurate as those obtained with the original $\overline{\tau}_j - \overline{\tau} - D_{50j}$ relations (Figure S3), although a larger number of events were underpredicted.

Text S8: Prediction and measurements uncertainties

Even though our predictions represent an improvement over other published methods, only about 50% of the events were within a factor of 2 of the measured values. We made a number of simplifications that may have reduced the accuracy of our predictions. Our method does not route the sediment throughout the reach, which may affect the predictions because fine and coarse fractions of the bedload can be routed over different paths [*Clayton and Pitlick*, 2007]. We assumed that patches were stable throughout every hydrograph, and even more, during each data set. We did not change the bed topography, patch area or the grain size distribution even when some events were more than one year apart (in the 2010 data).

One particular source of uncertainty is the simplified term for sediment supply. In steep mountain channels, sediment supply is primary driven by episodic landslides and debris flows (e.g., *Bathurst et al.* [1986]; *Benda and Dunne* [1997]) and is sensitive to human activities in a watershed [*Yu et al.*, 2009], the presence and severity of wildfires [*Benda et al.*, 2003; *Goode et al.*, 2012], hillslope processes (i.e. degree of vegetation, [*Recking*, 2012]), and seasonal

194 variations. We lack a mechanism to predict the exact timing and caliber of material that a
195 landslide or debris flow delivers, and explicitly including them in bed load calculations is not
196 feasible. We partially overcome this issue by using the protrusion of the immobile steps, as a
197 proxy for sediment supply [*Yager et al.*, 2012b], . Other important mechanisms, such as bed
198 scour, sediment deposition, shear stress divergence, flow turbulence and hydrograph effects, were
199 omitted in our study. Explicitly including them could improve future sediment transport
200 predictions. Other potential sources of uncertainties come from our measured values of water
201 surface elevation and the stage-discharge relation, especially for high discharges. Fluctuations in
202 the observed water surface elevations indicate that there were local and temporal flow
203 unsteadiness that the hydrodynamic model was not able to capture.

204 We used a sediment transport equation developed using reach-averaged properties (e.g. $\overline{\tau}$ and
205 D_{50}) and applied it at the patch scale. We divided each patch into 25 sub-areas, which gave an
206 average sub-area of 0.55 and 0.93 m^2, for the 2010 and 2011 data sets, respectively, with a
207 minimum of approximately 0.05 m^2. Although no study, to the best of our knowledge, has
208 defined the finest scale at which a certain sediment transport equation is applicable, most 2D and
209 3D models with sediment transport capabilities use a grid based algorithm. This approach has
210 been successfully applied using finer or similar grid sizes to that used in this study. For example,
211 sediment transport calculations has been used in numerical simulations of flume experiments
212 using the STREMR HySeD model [*Abad et al.*, 2008] and field applications using the RMA2
213 [*King*, 1990; *Rathburn and Wohl*, 2003] and also the FaSTMECH models [*Maturana et al.*,
214 2014].
215

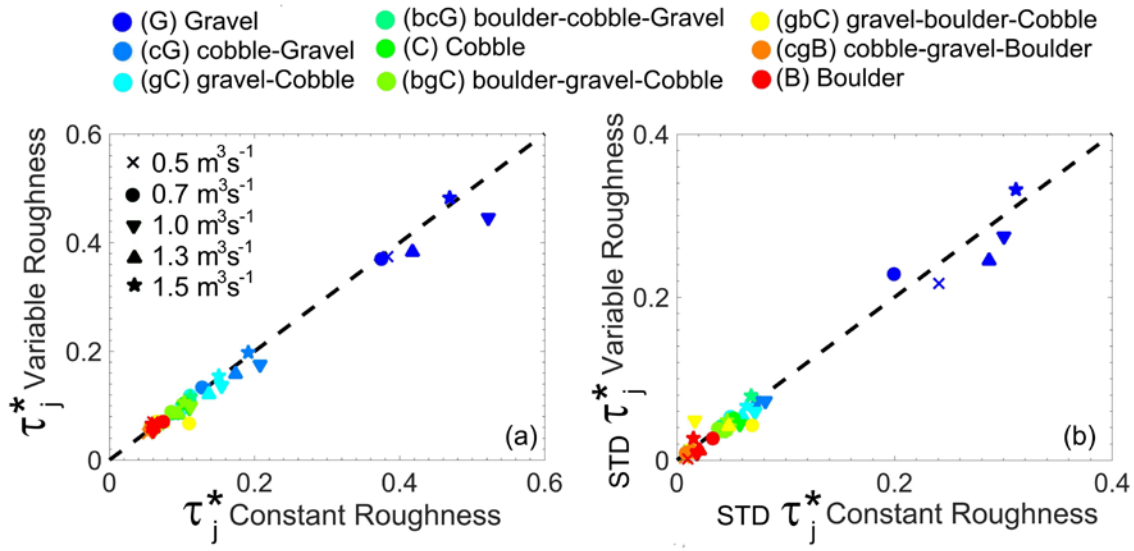

Figure S1: Comparison between the predicted (a) dimensionless mean shear stress class and (b) standard deviation for each patch using a spatially constant or variable drag coefficient . A representative set of discharge for the 2010 data sets are shown. Markers have been colored by patch class while different shapes have been used for discharge.

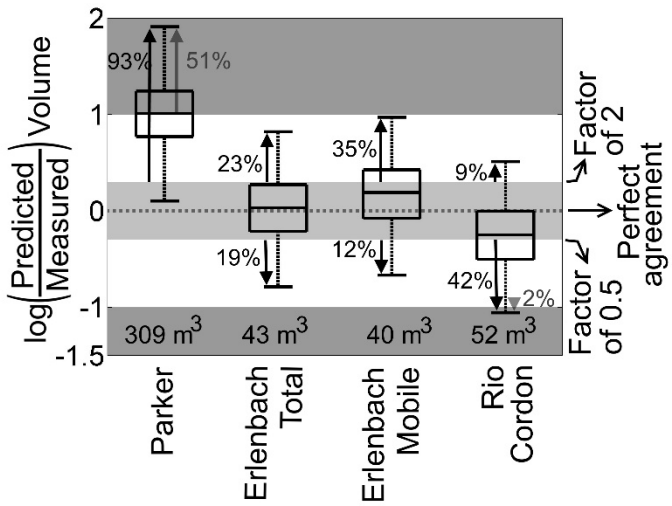

Figure S2: The log of the ratio of the predicted to measured sediment volume when different hiding functions are used. "Parker" is the original hiding function of *Parker* [1990], "Erlenbach Total" and "Erlenbach Mobile" are those obtained by *Yager et al.* [2012a] and use the total bed grain size distribution and only the mobile grain fraction, respectively. "Rio Cordon" is the hiding function for the Rio Cordon [*Mao and Lenzi*, 2007]. See Figure 7 in the main text for other figure details.

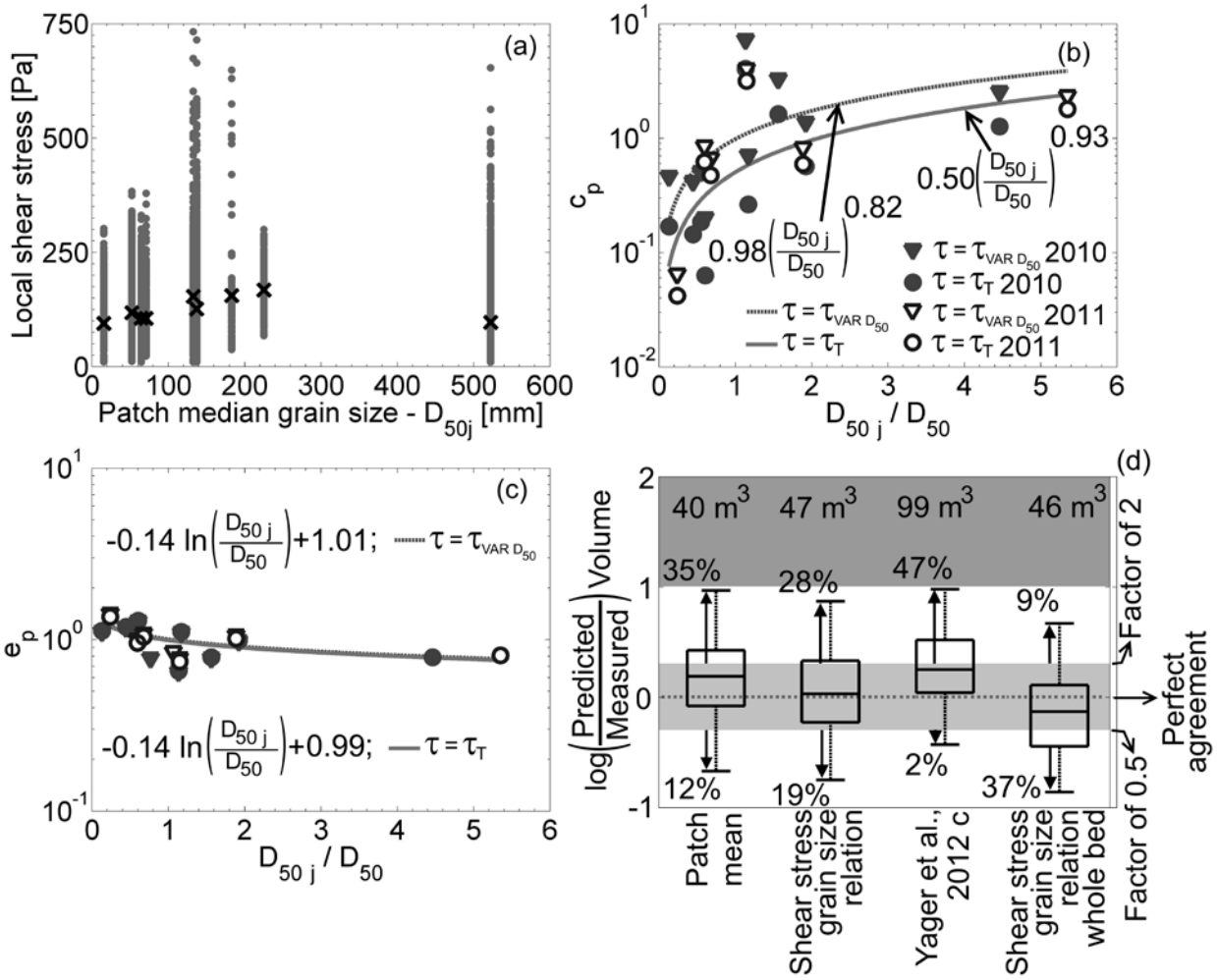

Figure S3: Shear stress and sediment transport predictions using the whole wetted surface. (a) Local boundary shear stress versus local median surface grain size for a discharge of 1 m^3/s for the 2010 data set and the whole wetted bed surface. Each circle represents a wetted node in the numerical model. Relations of (b) the coefficient and (c) exponent in equations (S5) and (S6). (d) Sediment transport volume predictions using equations (S5) and (S6) compared to those obtained by the "Patch mean", the original $\overline{\tau}_j - \overline{\tau} - D_{50\,j}$ relations and *Yager et al*. [2012 c]. See Figure 7 for an explanation of the box properties.

	Percentage of events where the observed shear stresses comes from the hypothesized continuous distribution with statistically confidence				
Data Sets	Normal	Lognormal	Gamma	GEV	Exponential
2010	12.61	17.72	18.62	18.62	1.20
2011	3.90	12.31	6.91	11.11	4.20

Table S1. Performance of the continuous probability distribution to predict the observed (from the model) shear stress distributions. Each event correspond to a specific patch class and discharge. 2010 and 2011 correspond to the two data sets analyzed

244

Hiding Function	Hiding Function Coefficient	Hiding Function Exponent
Parker	0.0386	-0.9049
Erlenbach - Total bed	0.14	-0.62
Erlenbach - Mobile	0.07	-0.16
Rio Cordon	0.189	-0.639

245 Table S2. Hiding functions used in bed load calculations

246
247

248

Parameter	2010	2011	2004	2004 source
S (%)	9.9	9.8	9.8	Ref 2
w (m)	4.7	4.7	4.7	Ref 1; Ref 2
A_m/A_T	0.70	0.74	0.67	Ref 2
z_{mu} (mm)	310	302	310	Ref 1
p_u(mm)	144	110	130	Ref 1
D (mm)	454	412	442	Ref 2
D_{84} (mm)	n/r	n/r	494	Ref 2
D_{90} (mm)	n/r	n/r	619	Ref 3
λ_X (m)	4.0	4.0	4.0	Ref 1
λ_W (m)	1.3	1.3	1.3	Ref 1
C_m	0.44	0.44	0.44	Ref 1
w_{bottom} (m)	n/r	n/r	3.5	Ref 1
L (m)	n/r	n/r	7.86	Ref 1
H (m)	n/r	n/r	0.69	Ref 1
KE	n/r	n/r	0.48	Ref 1
a	n/r	n/r	2.5	Ref 1
α	n/r	n/r	0.14	Ref 1

249 Table S3: Field measurements used to predict reach-averaged velocity and sediment transport
250 rates, "m" denotes the relatively mobile sediment. Parameters are proportion of the bed covered
251 by mobile sediment (A_m/A_T), the depth of the mobile sediment (z_{mu}), the immobile-grain:
252 protrusion (p_u), mean diameter (D), downstream spacing (λ_X), and downstream length (λ_W), D_{84}
253 and D_{90} are the 84^{th} and 90^{th} percentile grain sizes, w is the channel width, w_{bottom} is the bottom
254 width, L and H are the mean step length and height, respectively, KE and a are parameters in the

255 Egashira and Ashida [1991] equation, α is the block concentration. “n/r” stands for not required
256 for sediment transport predictions using the corresponding method (see text for details). Ref1,
257 Ref2 and Ref3 are *Nitsche et al*. [2011], *Yager et al*. [2012a], and *Yager et al*. [2012b],
258 respectively.
259

References

Abad, J. D., G. C. Buscaglia, and M. H. Garcia (2008), 2D stream hydrodynamic, sediment transport and bed morphology model for engineering applications, *Hydrol. Process.*, *22*(10), 1443–1459, doi:10.1002/hyp.6697.

Bathurst, J. C., G. J. L. Leeks, and M. D. Newson (1986), Field measurements for hydraulic and geomorphological studies of sediment transport - The special problems of mountain streams, in *Proceedings of the International Symposium on Measuring Techniques in Hydraulic Research*, pp. 137–151, Balkema, Netherlands.

Benda, L., and T. Dunne (1997), Stochastic forcing of sediment routing and storage in channel networks, *Water Resour. Res.*, *33*(12), 2865–2880, doi:10.1029/97WR02387.

Benda, L., D. Miller, P. Bigelow, and K. Andras (2003), Effects of post-wildfire erosion on channel environments, Boise River, Idaho, *For. Ecol. Manage.*, *178*(1-2), 105–119, doi:10.1016/S0378-1127(03)00056-2.

Clayton, J. a., and J. Pitlick (2007), Spatial and temporal variations in bed load transport intensity in a gravel bed river bend, *Water Resour. Res.*, *43*, W02426, doi:10.1029/2006WR005253.

Fleiss, J. L., B. Levin, and M. C. Paik (2004), *Statistical Methods for Rates and Proportions*, 3rd ed., John Wiley & Sons, Inc., Hoboken, New Jersey, USA.

Goode, J. R., C. H. Luce, and J. M. Buffington (2012), Enhanced sediment delivery in a changing climate in semi-arid mountain basins: Implications for water resource management and aquatic habitat in the northern Rocky Mountains, *Geomorphology*, *139-140*, 1–15, doi:10.1016/j.geomorph.2011.06.021.

King, I. P. (1990), *Program Documentation: RMA2-A Two-Dimensional Finite Element Model for Flow in Estuaries and Streams. Ver 4.3. Resource Management Associates, Lafayette, CA.*

Lisle, T. E., J. M. Nelson, J. Pitlick, M. A. Madej, and B. L. Barkett (2000), Variability of bed mobility in natural, gravel-bed channels and adjustments to sediment load at local and reach

scales, *Water Resour. Res.*, *36*(12), 3743–3755, doi:10.1029/2000WR900238.

Mao, L., and M. A. Lenzi (2007), Sediment mobility and bedload transport conditions in an alpine stream, *Hydrol. Process.*, *21*(14), 1882–1891, doi:10.1002/hyp.6372.

Maturana, O., D. Tonina, J. A. McKean, J. M. Buffington, C. H. Luce, and D. Caamaño (2014), Modeling the effects of pulsed versus chronic sand inputs on salmonid spawning habitat in a low-gradient gravel-bed river, *Earth Surf. Process. Landforms*, *39*, 877–889, doi:10.1002/esp.3491.

Nelson, J. M., and J. D. Smith (1989), Flow in meandering channels with natural topography, in *River Meandering, Water Resources Monographs*, vol. 12, edited by S. Ikeda and G. Parker, pp. 69–102, American Geophysical Union, Washington, D.C., USA.

Nelson, P. A., W. E. Dietrich, and J. G. Venditti (2010), Bed topography and the development of forced bed surface patches, *J. Geophys. Res. Earth Surf.*, *115*, F04024, doi:10.1029/2010JF001747.

Parker, G. (1990), Surface-based bedload transport relation for gravel rivers, *J. Hydraul. Res.*, *28*(4), 417–436, doi:10.1080/00221689009499058.

Pasternack, G. B., A. T. Gilbert, J. M. Wheaton, and E. M. Buckland (2006), Error propagation for velocity and shear stress prediction using 2D models for environmental management, *J. Hydrol.*, *328*(1-2), 227–241, doi:10.1016/j.jhydrol.2005.12.003.

Rathburn, S., and E. Wohl (2003), Predicting fine sediment dynamics along a pool-riffle mountain channel, *Geomorphology*, *55*(1-4), 111–124, doi:10.1016/S0169-555X(03)00135-1.

Recking, A. (2012), Influence of sediment supply on mountain streams bedload transport, *Geomorphology*, *175-176*, 139–150, doi:10.1016/j.geomorph.2012.07.005.

Segura, C., and J. Pitlick (2015), Coupling fluvial-hydraulic models to predict gravel transport in spatially variable flows, *J. Geophys. Res. Earth Surf.*, *120*, 834–855, doi:10.1002/2014JF003302.

312 Whiting, P. J., and W. E. Dietrich (1991), Convective accelerations and boundary shear stress
313 over a channel bar, *Water Resour. Res.*, *27*(5), 783–796, doi:10.1029/91WR00083.
314 Yager, E. M., W. E. Dietrich, J. W. Kirchner, and B. W. McArdell (2012a), Prediction of
315 sediment transport in step-pool channels, *Water Resour. Res.*, *48*(1), 1–20,
316 doi:10.1029/2011WR010829.
317 Yager, E. M., J. M. Turowski, D. Rickenman, and B. W. McArdell (2012b), Sediment supply,
318 grain protrusion, and bedload transport in mountain streams, *Geophys. Res. Lett.*, *39*,
319 L10402, doi:10.1029/2012GL051654.
320 Yu, G., Z. Wang, K. Zhang, T. Chang, and H. Liu (2009), Effect of incoming sediment on the
321 transport rate of bed load in mountain streams, *Int. J. Sediment Res.*, *24*(3), 260–273,
322 doi:10.1016/S1001-6279(10)60002-9.
323

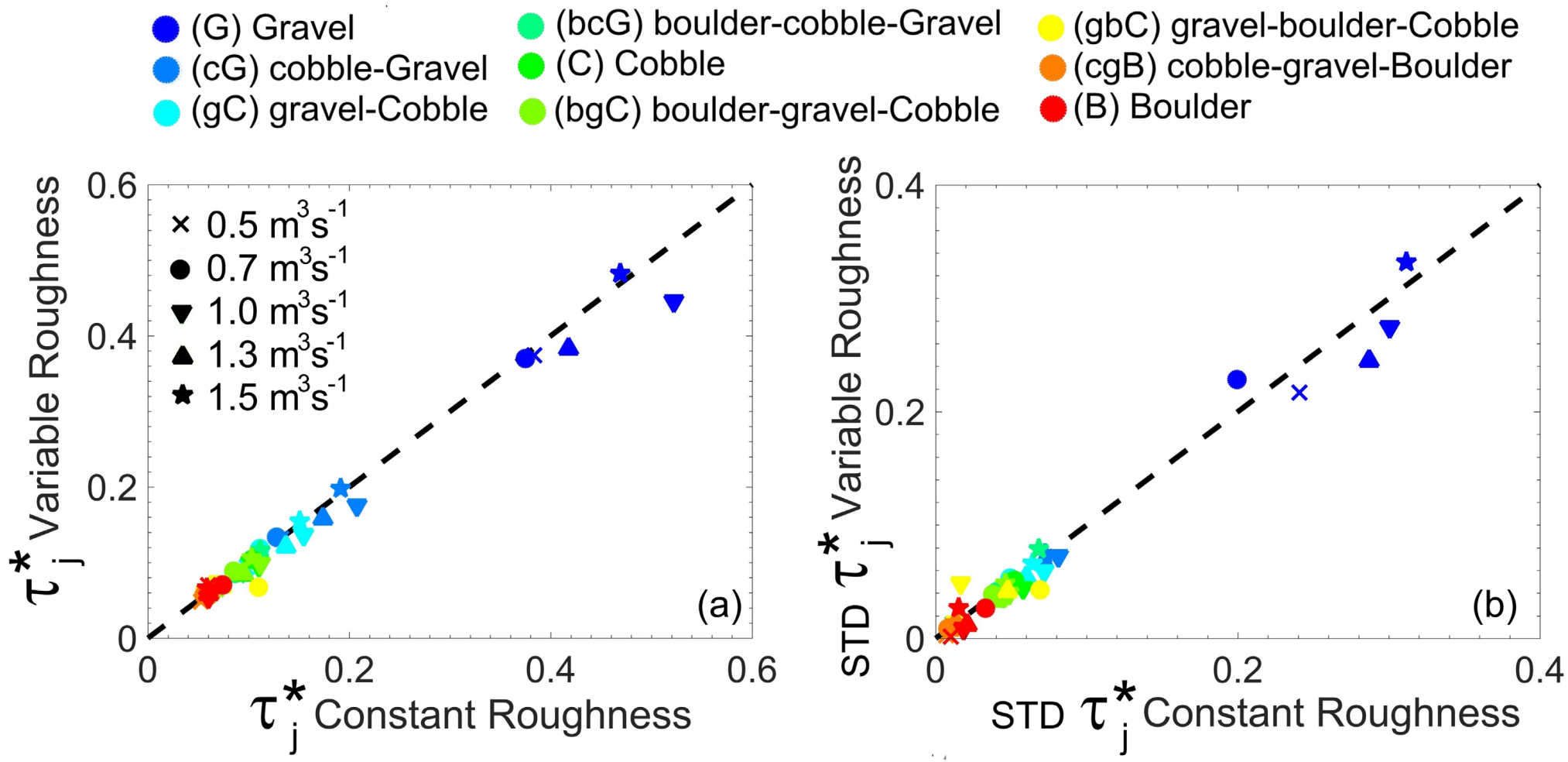

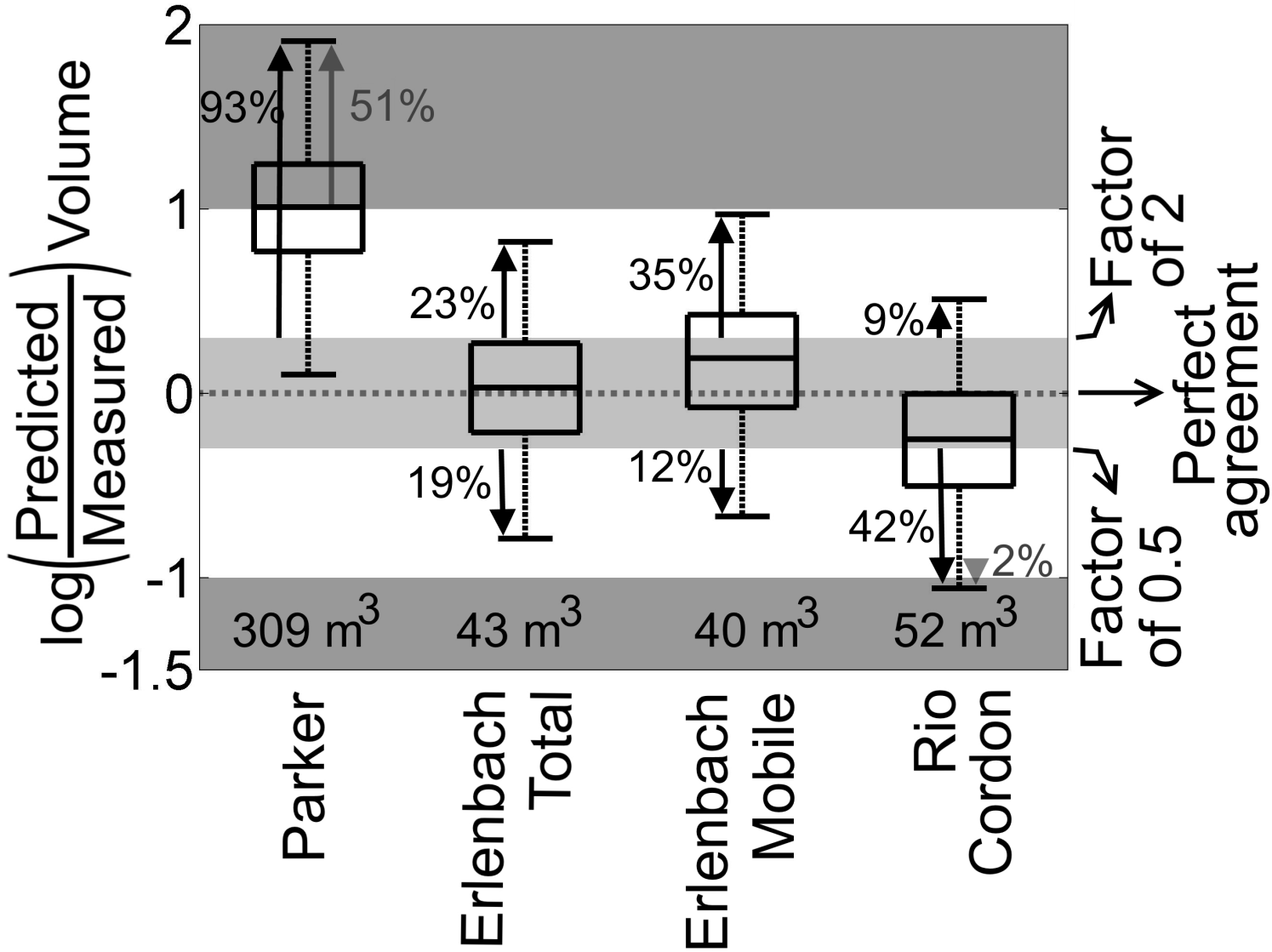

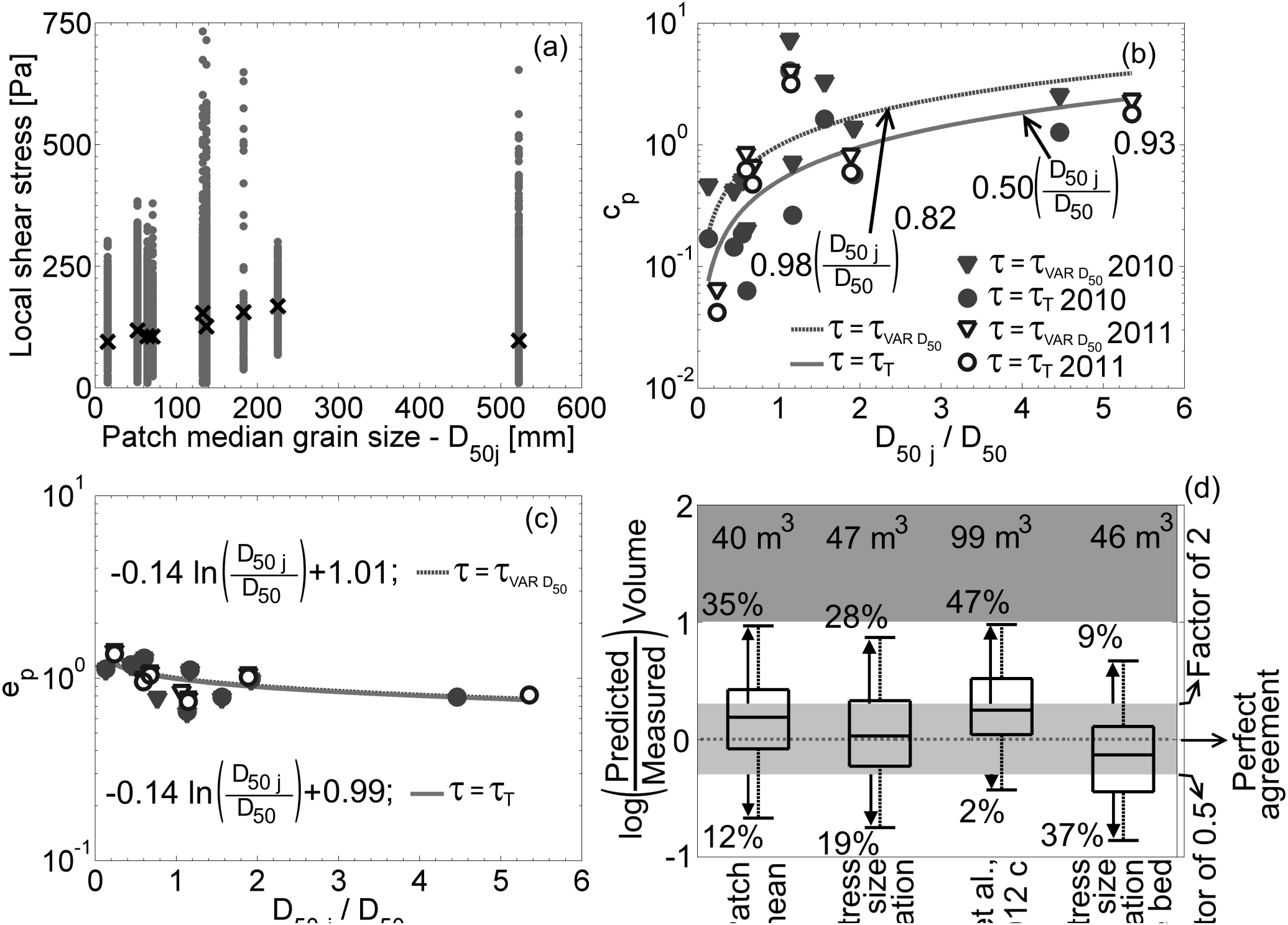
(a)
Local shear stress [Pa]
Patch median grain size - D_{50j} [mm]
(b)
c_p
$D_{50\,j} / D_{50}$
$0.98\left(\frac{D_{50\,j}}{D_{50}}\right)^{0.82}$
$0.50\left(\frac{D_{50\,j}}{D_{50}}\right)^{0.93}$
$\tau = \tau_{VAR\ D_{50}}$ 2010
$\tau = \tau_T$ 2010
$\tau = \tau_{VAR\ D_{50}}$ 2011
$\tau = \tau_T$ 2011
$\tau = \tau_{VAR\ D_{50}}$
$\tau = \tau_T$
(c)
e_p
$-0.14\ln\left(\frac{D_{50\,j}}{D_{50}}\right)+1.01$; $\tau = \tau_{VAR\ D_{50}}$
$-0.14\ln\left(\frac{D_{50\,j}}{D_{50}}\right)+0.99$; $\tau = \tau_T$
$D_{50\,j} / D_{50}$
(d)
$\log\left(\frac{\text{Predicted}}{\text{Measured}}\right)$ Volume
40 m^3
47 m^3
99 m^3
46 m^3
35%
28%
47%
9%
12%
19%
2%
37%
Factor of 2
Perfect agreement
Factor of 0.5

P
m

Shear st
grain
rela

Yager e
20

Shear st
grain
rela
whole

Fact